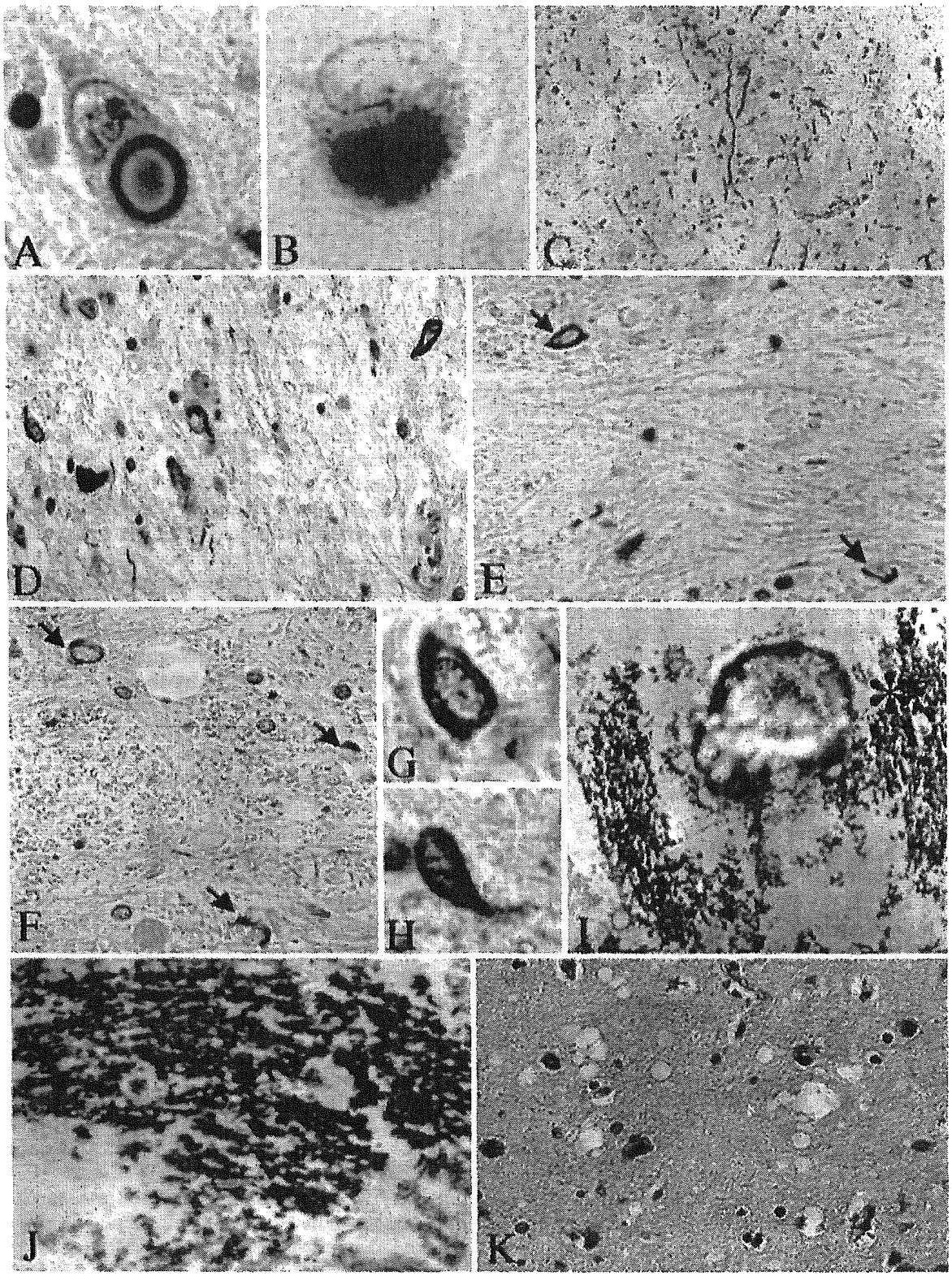

Fig. 3 A α-Synuclein-positive brain stem-type LB. B Ubiquitin positive cortical LB, which is also immunostained by anti-α-synuclein antibody. C In the CA2-3 sector of the hippocampus, numerous neuritic changes can be observed by α-synuclein immunostaining. D Coil-like inclusions in the substantia nigra. E Ubiquitin-positive glial inclusion in the medulla. F α-Synuclein-positive glial inclusion in the medulla. G Higher magnification of the ubiquitin-positive glial inclusion in the medulla. H Higher magnification of the α-synuclein-positive glial inclusion in the medulla. I Immunoelectron micrograph of α-synuclein-positive glial inclusion in putamen. J High-power view of the glial inclusion (*asterisk*) in I. K Spongiform changes within the temporal neocortex. A, C, F, H–J α-Synuclein immunostaining; B, E, G ubiquitin immunostaining; D Gallyas-Braak stain; K hematoxylin-eosin. A ×1,000; B ×900; C, K ×200; D–F ×400; G, H ×1,500; I ×8,000; J ×20,000

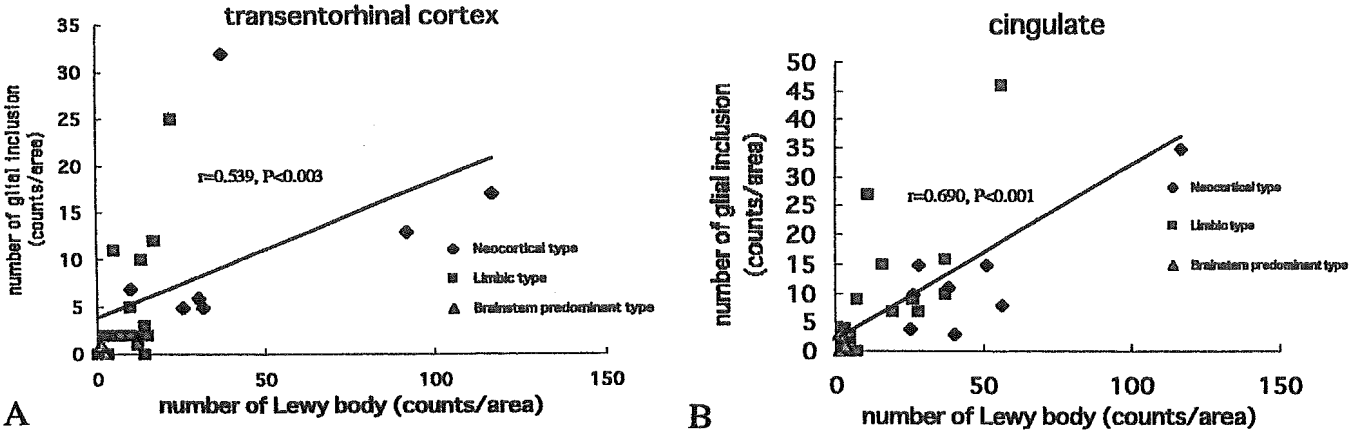

Fig. 4 Correlation of the total number of glial inclusions and LBs in the transentorhinal cortex (**A**) and anterior cingulated gyrus (**B**). Total inclusions counts correlate well to the total counts of LBs (transentorhinal cortex; r =0.539, P <0.003, and anterior cingulated gyrus; r =0.690, P <0.001). The areas of the transentorhinal cortex and anterior cingulated gyrus were defined according to [22]

Spongiform changes (microvacuolation)

Spongiform changes were found most frequently in the neocortical-type cases and were found only occasionally in the other two types of cases (Table 2) (Fig. 3K). Spongiform changes were largely restricted to the temporal neocortex, amygdale, and cingulate gyrus.

Clinical and pathological correlation

In this study, all neocortical type cases involved parkinsonism and dementia, and autonomic failure was noted in all cases examined. Dementia appeared within 1 year of the onset of parkinsonism in cases 2, 4, 6, and 7. Cases 1, 3, 5, and 8 also showed dementia, but this appeared more than 1 year after the onset of parkinsonism. Clinical diagnosis was DLB in 3 cases, PD with dementia in 3 cases, and Shy-Drager syndrome in 2 cases (Table 1).

All limbic type cases involved parkinsonism (Table 1). Twelve of 17 patients (70.6%) who were examined were demented. Severe and fluctuating cognition, and impairment of visuospatial performance were observed in 4 of these 12 cases (cases 15, 17, 21, 24). In all cases, the onset of dementia was more than 1 year after the appearance of parkinsonism. There was no sign of dementia in 7 cases, and, in 9 of 16 patients (56.2%) who could be examined, autonomic failure was seen. The clinical diagnosis was PD with dementia in 12 cases, PD in 6, and Shy-Drager syndrome in 1.

All of the brain stem-predominant type cases involved symptom of autonomic failure. There was only one case that involved parkinsonism that carried a diagnosis of PD. Two other cases that had no sign of parkinsonism carried a diagnosis of PAF. Dementia was not noted in any of the brain stem-type cases (Table 1).

Discussion

Theappearance of LBs is a common neuropathological feature and a principal hallmark of both PD and DLB; LBs are also found in PAF [11]. LBs are eosinophilic neuronal inclusion bodies, with α-synuclein being a major component [14, 28]. There have been several resent studies showing that cytoplasmic aggregation of α-synuclein also occurs in glial cells in the brains of both PD and DLB patients [2, 12, 32, 33]. These inclusions can be distinguished from glial fibrillary tangles, glial cytoplasmic inclusions, and coiled bodies by their distribution pattern, shape, α-synuclein positivity, tau protein negativity, and presence in both oligodendroglia and astrocytes. However, the frequency and precise distribution of such glial inclusions and their relation to the presence of LBs have not yet been clarified. Thus, we investigated the relation between the distribution pattern of α-synuclein aggregates in neurons and glial cells and the clinical phenotypes.

We confirmed that aggregation of α-synuclein occurred in both neurons and glial cells in all cases of LB disease. The pattern of LBs distribution in the cerebral cortex differed among the three pathological types. The distribution pattern in the brain stem and spinal cord, however, was quite similar among the three types. All 30 cases showed abundant coil-like glial inclusions to various degrees, and these were distributed extensively in the cerebral cortex, white matter of the cerebrum and cerebellum and the spinal cord, and most frequently in the brain stem. In our study, we used 8-μm-thick sections for G-B staining and immunocytochemistry, and performed formic acid pretreatment, which markedly enhanced α-synuclein immunoreactivity. This treatment is suggested to enhance the glial inclusions, and in the present study these were found to be more widespread than has been reported previously.

In any given individual, the distributions of LBs and coil-like glial inclusions were similar in the brain stem and cerebral cortex independent of types of pathological classification. The underlying pathological basis for this parallel distribution of LBs and glial inclusions is unknown, but we can speculate that glial inclusions are related pathogenically to the process of LB formation. Abeliovich et al. [1] recently reported that α-synuclein-defi-

cient mice show a reduction in striatal dopamine and decreased dopamine-dependent locomotor response to amphetamine, leading them to speculate that α-synuclein provides functional support to dopaminergic neurons. In our study, the distribution of inclusion-bearing neurons and glial cells in LB disease corresponded well to the distribution of catecholaminergic neurons and fibers, particularly in the brain stem region, the region most severely involved [8, 26]. We suspect that the appearance of LBs and glial inclusions is associated in some way with damage to the catecholaminergic neurons.

The clinical features of the three types of LB disease bore a close resemblance in our autopsy cases. Several studies have shown extensive overlap between the clinical features of PD with or without dementia and DLB: resting tremor, rigidity, akinesia, progressive cognitive decline, memory disturbance, and orthostatic hypotension, for example [6, 13, 16, 20]. The clinical data in this study were limited to evidence of dementia (based on clinical neurological, psychiatric, and neuropsychological evaluations and often included mini-mental examination), of parkinsonism (based on the presence of extrapyramidal signs), and of autonomic failure (based on the presence of orthostatic hypotension, or low uptake of metaiodobenzylguanidine myocardial scintigraphy). All neocortical type cases included evidence of parkinsonism, dementia, and autonomic failure during the patient's lifetime. Some subjects showed dementia very early (within 1 year), others developed dementia late (final 1–2 years) in the disease course. Neuropathologically, there was no difference between these cases in terms of brain weight, spongiform change, or the distribution of LBs and glial inclusions. The limbic-type group (cases 12, 14, 15, 16, 17, 22, 24) with an LB score 6, suffered from parkinsonism, autonomic failure, and dementia (sometimes with fluctuating cognitive decline), and the clinical features in this group resembled those of the neocortical-type cases. However, in cases 18, 19, 20, 23, which involved parkinsonism without psychiatric sings, the LBs score ranged from 3 to 5, and LB and glial inclusion counts within the five areas tended to less than those of cases suffering from both parkinsonism and dementia. None of the brain stem-type patients were demented during their lifetime, but all showed severe autonomic failure. Each LB score was 2, and the number of LB and glial inclusions within the cerebral cortex were very small, and close those of PD cases without dementia. From our findings we believe that neocortical LBs and glial inclusions, particularly in the limbic cortex, are responsible for the appearance of dementia, irrespective of the three classifications. No apparent relationship between parkinsonism or autonomic failure and the patterns of LB and glial inclusion distribution was observed, but because autonomic failure was seen in parallel with the brain stem or spinal cord lesion, it is reasonable that common pathological processes among these three disease types could contribute to the symptoms of autonomic failure.

We had no case of the "cerebral type", reported by Kosaka et al. [18, 19]. It seems that LBs can occur anywhere in the cerebral cortex, brain stem, and spinal cord, but that the distribution and density of LBs differs from case to case. The relationship between the occurrence of LBs and coil-like glial inclusions, and neuronal death is not yet clear, but it is clear that LBs and glial inclusions are found predominantly in the affected region, and that such degeneration affects clinical expression.

We conclude that DLB, PD with or without dementia, and PAF share several clinical and neuropathological features. It seems reasonable to regard these conditions as part of a disease spectrum, i.e., the "LB disease" spectrum. Further study is needed to elucidate the underlying pathological mechanism for the related appearance of LBs, glial inclusions, and loss of neurons in LB disease.

References

1. Abeliovich A, Schmitz Y, Farinas I, Choi-Lundberg D, Ho WH, Castillo PE, Shinsky N, Verdugo JM, Armanini M, Ryan A, Hynes M, Phillips H, Sulzer D, Rosenthal A (2000) Mice lacking α-synuclein display functional deficits in the nigrostriatal dopamine system. Neuron 25:239–252
2. Arai T, Ueda K, Ikeda K, Akiyama H, Haga C, Kondo H, Kuroki N, Niizato K, Iritani S, Tsuchiya K (1999) Argyrophilic glial inclusions in the midbrain of patients with Parkinson's disease and diffuse Lewy body disease are immunopositive for NACP/α-synuclein. Neurosci Lett 259:83–86
3. Arima K, Ueda K, Sunohara N, Hirai S, Izumiyama Y, Tonozuka-Uehara H, Kawai M (1998) Immunoelectron-microscopic demonstration of NACP/α-synuclein-epitopes on the filamentous component of Lewy bodies in Parkinson's disease and in dementia with Lewy bodies. Brain Res 808:93–100
4. Baba M, Nakajo S, Tu PH, Tomita T, Nakaya K, Lee VMY, Trojanowski JQ, Iwatsubo T (1998) Aggregation of α-synuclein in Lewy bodies of sporadic Parkinson's disease and dementia with Lewy bodies. Am J Pathol 152:879–884
5. Braak E, Braak H (1991) Neuropathological stageing of Alzheimer-related changes. Acta Neuropathol 82:239–259
6. De Vos RA, Jansen EN, Atam FC, Ravid R, Swaab DF (1995) 'Lewy body disease': clinico-pathological correlations in 18 consecutive cases of Parkinson's disease with and without dementia. Clin Neurol Neurosurg 97:13–22
7. Dickson DW, Ruan D, Crystal H Mark MH, Davies P, Kress Y, Yen SH (1991) Hippocampal degeneration differentiates diffuse Lewy body disease (DLDB) from Alzheimer's disease: light and electron microscopic immunocytochemistry of CA 2–3 neurites specific to DLBD. Neurology 41:1402–1409
8. German DC, Manaye K, Smith WK, Woodward DJ, Saper CB (1989) Midbrain dopaminergic cell loss in Parkinson's disease: computer visualization. Ann Neurol 26:507–514
9. Halliday GM, Li YW, Blumbergs PC, Joh TH, Cotton RGH, Howe PRC, Blessing WW, Geffen LB (1990) Neuropathology of immunohistochemically identified brainstem neurons in Parkinson's disease. Ann Neurol 27:373–385
10. Hansen LA, Masliah E, Terry RD, Mirra SS (1989) A neuropathological subset of Alzheimer's disease with concomitant Lewy body disease and spongiform change. Acta Neuropathol 78:194–201
11. Hishikawa N, Hashizume Y, Hirayama M, Imamura K, Washimi Y, Koike Y, Mabuchi C, Yoshida M, Sobue G (2000) Brainstem-type Lewy body disease presenting with progressive autonomic failure and lethargy. Clin Autonom Res 10:139–143
12. Hishikawa N, Hashizume Y, Yoshida M, Sobue G (2001) Widespread occurrence of argyrophilic glial inclusions in Parkinson's disease. Neuropathol Appl Neurobiol 27:362–372

13. Hughes AJ, Daniel SE, Kilford L, Lees AJ (1992) Accuracy of clinical diagnosis of idiopathic Parkinson's disease: a clinico-pathological study of 100 cases. J Neurol Neurosurg Psychiatry 55:181–184
14. Irizarry MC, Growdon W, Gomez-Isla T, Newell K, George JM, Clayton DF, Hyaman BT (1998) Nigral and cortical Lewy bodies and dystrophic nigral neurites in Parkinson's disease and cortical Lewy body disease contain α-synuclein immunoreactivity. J Neuropathol Exp Neurol 57:334–337
15. Iseki E, Li F, Odawara T, Kosaka K (1997) Hippocampal pathology in diffuse Lewy body disease using ubiquitin-immunohistochemistry. J Neurol Sci 149:165–169
16. Iseki E, Marui W, Kosaka K, Kato M, Yamamoto T, Ueda K (1999) Clinicopathological multiplicity of dementia with Lewy bodies. Neuropathology 19:386–394
17. Jellinger K (1986) Overview of morphological changes in Parkinson's disease. Adv Neurol 45:1–18
18. Kosaka K (1995) Diffuse Lewy body disease. Clin Neurol 35: 1455–1456
19. Kosaka K, Iseki E, Odawara T, Yamamoto T (1996) Cerebral type of Lewy body disease. Neuropathology 16:32–35
20. Kosaka K, Matsushima M, Oyanagi S, Mehraein P (1980) A clinicopathological study of the "Lewy body disease". Psychiatr Neurol Jpn 82:292–311
21. Mann DMA, Yates PO (1983) Pathological basis for neurotransmitter changes in Parkinson's disease. Neuropathol Appl Neurobiol 9:3–19
22. McKeith IG, Galasko D, Kosaka K, Perry EK, Dickson DW, Hansen LA, Salmon DP, Lowe J, Mirra SS, Byrne EJ, Lennox G, Quinn NP, Edwardson JA, Ince PG, Bergeron C, Burns A, Miller BL, Lovestone S, Collerton D, Jansen ENH, Ballard C, Vos RA de, Wilcock GK, Jellinger KA, Perry RH (1996) Consensus guidelines for the clinical and pathological diagnosis of dementia with Lewy bodies (DLB): report of the consortium on DLB international workshop. Neurology 47:1113–1124
23. Mirra SS, Heyman A, McKeel D, Sumi SM, Crain BJ, Brownlee LM, Vogel FS, Hughes JP, Belle G van, Berg L, participating CERAD neuropathologists (1991) The Consortium to Establish a Registry for Alzheimer's Disease (CERAD). Part II. Standardization of the neuropathologic assessment of Alzheimer's disease. Neurology 41:479–486
24. Morris CM, Candy JM, Bloxham CA, Edwardson JA (1992) Immunocytochemical localization of transferrin in the human brain. Acta Anat (Basel) 143:14–18
25. Murray AM, Weihmueller FB, Marshall JF, Hurtig HI, Gottleib GL, Joyce JN (1995) Damage to dopamine systems differs between Parkinson's disease and Alzheimer's disease with parkinsonism. Ann Neurol 37:3200–317
26. Pearson J, Goldstein M, Markey K, Brandeis L (1983) Human brain stem catecholamine neuronal anatomy as indicated by immunocytochemistry with antibodies to tyrosine hydroxylase. Neuroscience 8:3–32
27. Piao YS, Wakabayashi K, Hayashi S, Yoshimoto M, Takahashi H (2000) Aggregation of α-synuclein/NACP in the neuronal and glial cells in diffuse Lewy body disease: a survey of six patients. Clin Neuropathol 19:163–169
28. Spillantini MG, Schmidt ML, Lee VMY, Trojanowski JQ, Jakes R, Hasegawa M, Goedert M (1997) α-Synuclein in Lewy bodies. Nature 388:839–840
29. Spillantini MG, Crowther RA, Jakes R, Hasegawa M, Goedert M (1998) α-Synuclein in filamentous inclusions of Lewy bodies from Parkinson's disease and dementia with Lewy bodies. Proc Natl Acad Sci USA 95:6469–6473
30. Terada S, Ishizu H, Haraguchi T, Takehisa S, Tanabe Y, Kawai K, Kuroda S (2000) tau-negative astrocytic star-like inclusions and coiled bodies in dementia with Lewy bodies. Acta Neuropathol 100:464–468
31. Tu PH, Galvin JE, Baba M, Giasson B, Tomita T, Leight S, Nakajo S, Iwatsubo T, Trojanowski JQ, Lee VM-Y (1998) Glial cytoplasmic inclusions in white matter oligodendrocytes of multiple system atrophy brains contain insoluble α-synuclein. Ann Neurol 44:415–422
32. Wakabayashi K, Takahashi H (1996) Gallyas-positive, tau-negative glial inclusions in Parkinson's disease midbrain. Neurosci Lett 217:133–136
33. Wakabayashi K, Hayashi S, Yoshimoto M, Kudo H, Takahashi H (2000) NACP/α-synuclein-positive filamentous inclusions in astrocytes and oligodendrocytes of Parkinson's disease brains. Acta Neuropathol 99:14–20

Reprinted from JOURNAL OF NEUROLOGY, NEUROSURGERY & PSYCHIATRY, April 2003, Vol 74, No 4, p 423-426

PAPER

Onset age and severity of motor impairment are associated with reduction of myocardial ^{123}I-MIBG uptake in Parkinson's disease

K Hamada, M Hirayama, H Watanabe, R Kobayashi, H Ito, T Ieda, Y Koike, G Sobue

J Neurol Neurosurg Psychiatry 2003;**74**:423–426

See end of article for authors' affiliations

Correspondence to: Dr G Sobue, Department of Neurology, Nagoya University Graduate School of Medicine, Nagoya 466–8550, Japan; sobueg@med.nagoya-u.ac.jp

Received 18 August 2002
In revised form 2 December 2002
Accepted 3 December 2002

Objectives: To elucidate the factors associated with severity of cardiac sympathetic nerve involvement in idiopathic Parkinson's disease (PD).
Methods: ^{123}I-metaiodobenzylguanidine uptake was examined in 88 patients with PD. The ratio of the uptake in the heart (*H*) to that in the mediastinum (M) (the *H/M* ratio) was calculated and correlated with age at onset, age at examination, and disease severity and duration. Twenty five healthy people were also examined as a control.
Results: There was a mild but significant negative correlation between *H/M* ratio and age at onset (early, $r = -0.33$, $p = 0.002$; delayed, $r = -0.34$, $p = 0.001$) and between Hoehn and Yahr (H-Y) stage (early, $r = -0.30$, $p = 0.006$; delayed, $r = -0.32$, $p = 0.003$). There was no significant correlation between disease duration and *H/M* ratio. When patients with PD were classified into four subgroups on the basis of age at onset (> 62 or < 62 years) and disease severity (H-Y > III or H-Y ≤ II), the median *H/M* ratio of the older and more severe group was significantly lower than that of the younger and less severe group ($p = 0.005$).
Conclusion: This study suggests that late onset, high severity PD is associated with myocardial sympathetic dysfunction.

^{123}I-metaiodobenzylguanidine (MIBG) is a physiological analogue of noradrenaline that traces the uptake and transport of noradrenaline in presynaptic sympathetic nerve terminals and subsequent vesicular storage.[1] Myocardial MIBG scintigraphy has been used to evaluate cardiac sympathetic nerve endings in both cardiac and various neurological diseases.[2–5] In idiopathic Parkinson's disease (PD), myocardial MIBG uptake is significantly reduced even without apparent autonomic failure, which enables early diagnosis of the illness.[6–17] Several studies involving small numbers of patients have suggested that duration and severity influence MIBG uptake in PD.[12 13 15] However, the factors proposed to be involved differ with the report. Furthermore, no previous study has investigated the effect of age at onset on MIBG cardiac uptake. In the present study, we examined the relations between myocardial MIBG uptake and age at onset, age at examination, disease severity, and disease duration in 88 patients with PD.

PATIENTS AND METHODS

From January 1997 to October 2001, myocardial MIBG scintigraphy was performed in 100 patients with PD according to the criteria of the United Kingdom Brain Bank.[18] None of the patients had familial or past histories of heart disease. All patients were examined by routine brain magnetic resonance imaging, and these results were incorporated into the diagnosis. Patients with Parkinson-plus syndrome or drug induced and postencephalitic parkinsonism were excluded. Twelve of the 100 patients with PD onset before reaching 45 years of age were excluded to differentiate autosomal recessive juvenile parkinsonism.[19] Thus, 88 patients with PD with the following characteristics were studied: 54 men and 34 women; mean (SD) age of onset 63.5 (9.6) years, range 45–85 years; mean age at examination 68.0 (9.0) years, range 49–87 years; mean disease duration 4.6 (3.6) years, range 1–12 years; and mean L-dopa intake 259 (174) mg. The Hoehn and Yahr (H-Y) scale was used to assess the severity of motor impairment: 10, 27, 40, 9, and 2 subjects were classified into stages I, II, III, IV, and V, respectively, when cardiac MIBG uptake was assessed. As a control group, 25 age matched people with no history of neurological or heart disease (13 men and 12 women, age at examination 66.6 (9.3) years) were enrolled in this study. We obtained informed consent from all subjects.

The 88 patients with PD were subgrouped based on the following cut off values: < 62 years old (younger), > 62 years old (older), H-Y ≤ II (mild), and H-Y > III (severe). Postural impairment is thought to result from a combined effect of the disease and aging processes, suggesting the widespread involvement of subcortical structures.[20] Consequently, patients with PD were classified into four groups: older/severe, older/mild, younger/severe, and younger/mild.

^{123}I-MIBG (111 mBq) was injected intravenously into each subject. The early image of cardiac uptake was taken 15 minutes later and the delayed image three or four hours later. Regions of interest were placed on the whole heart and mediastinum of the front image. The ratio of ^{123}I-MIBG uptake in regions of interest of the heart to that in the mediastinum (*H/M* ratio) was calculated. The *H/M* ratios from early and delayed images were evaluated in this study.

The Mann-Whitney U test was used for examining the intentional difference between two groups, the Kruskal-Wallis test was used for examining the intentional difference between three groups, and then Scheffé's F was used for post hoc testing. The relations between *H/M* ratio and age at onset, age at examination, and disease duration were analysed using Pearson's correlation coefficient. The relation between *H/M* ratio and H-Y scale was analysed using Spearman's correlation coefficient. Calculations were performed using the statistical

Abbreviations: H-Y, Hoehn and Yahr; MIBG, ^{123}I-metaiodobenzylguanidine; PD, Parkinson's disease

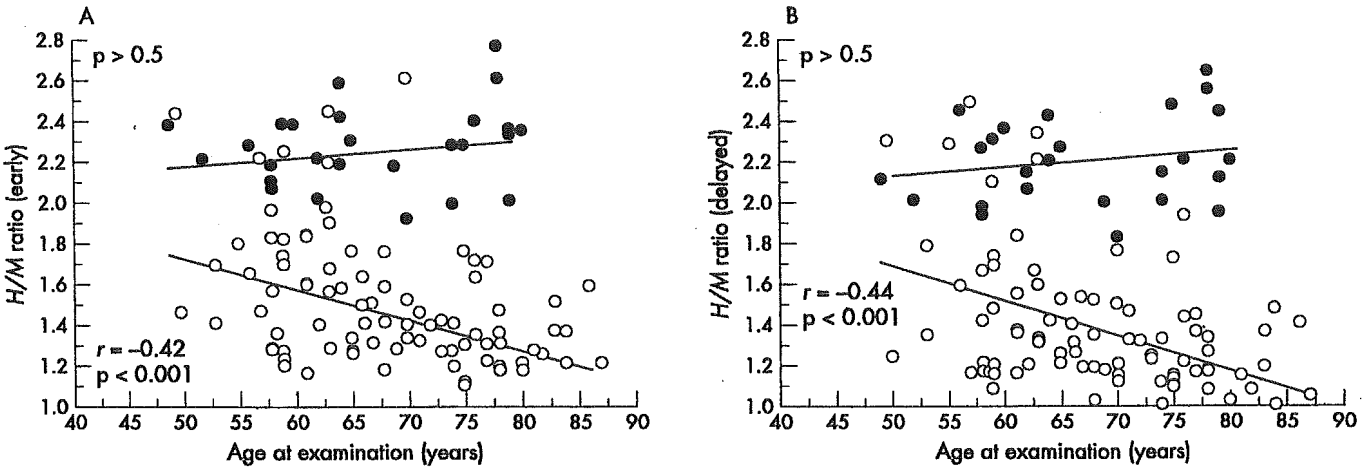

Figure 1 Age at examination had a significant negative correlation with heart to mediastinum (*H/M*) ratio in Parkinson's disease (PD) (PD patients: (A) early, $r = -0.42$, $p < 0.001$; (B) delayed $r = -0.44$, $p < 0.001$) but not in controls ($p > 0.5$). Open and closed circles represent individual patients with PD and control subjects, respectively.

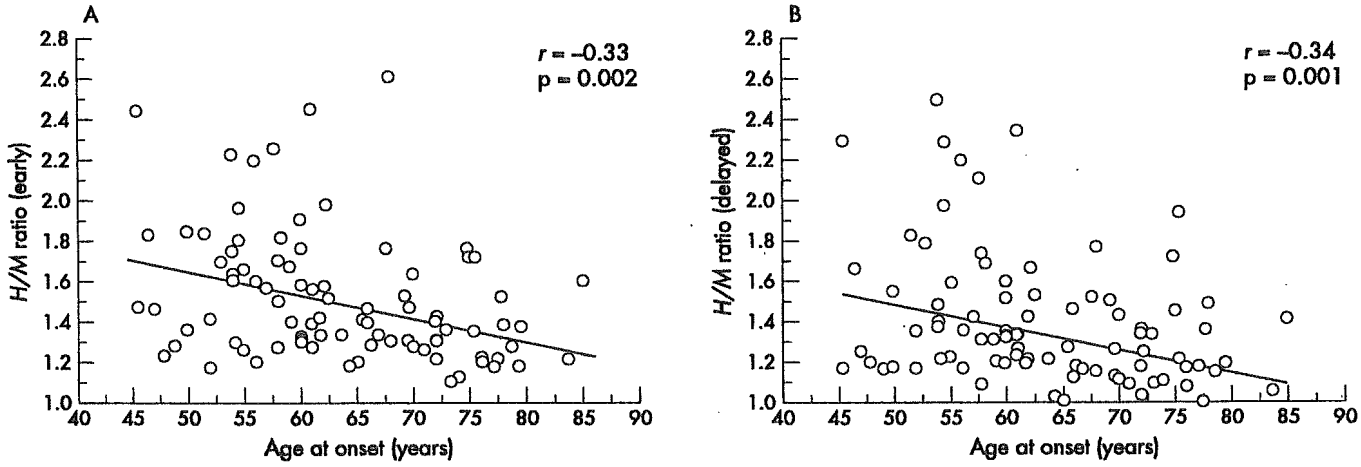

Figure 2 Age at onset had a slight but significant negative correlation with *H/M* ratio ((A) early, $r = -0.33$, $p = 0.002$; (B) delayed, $r = -0.34$, $p = 0.001$). Circles represent individual patients with PD.

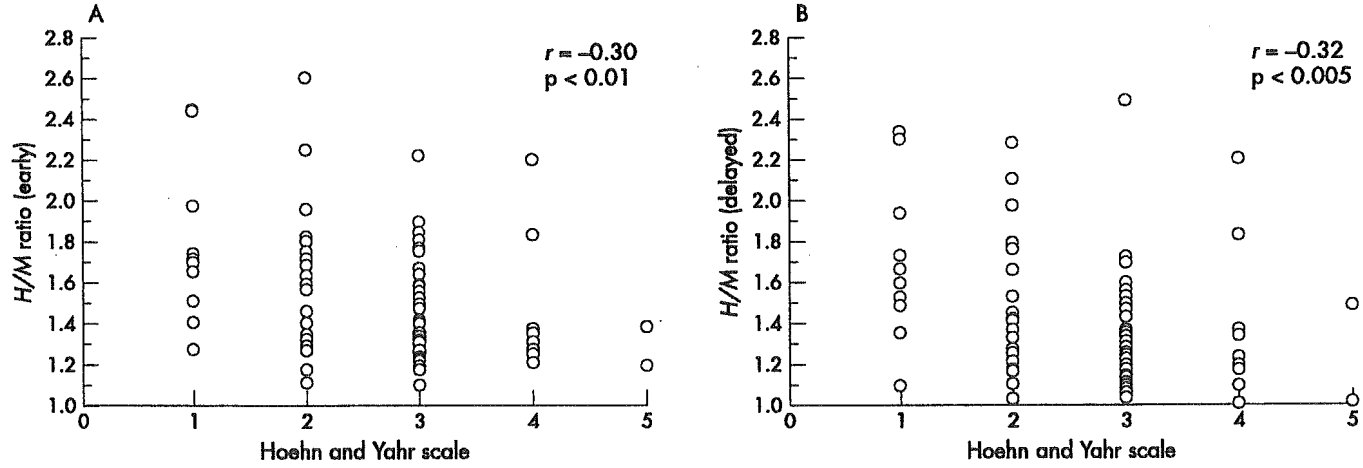

Figure 3 Hoehn and Yahr score had a slight but significant negative correlation with *H/M* ratio ((A) early, $r = -0.30$, $p < 0.01$; (B) delayed, $r = -0.32$, $p = 0.005$). Circles represent individual patients with PD.

software package StatView (Abacus Concepts, Berkeley, California, USA). The level of significance was defined at $p < 0.05$.

RESULTS

The *H/M* ratio of all patients with PD was significantly reduced compared with controls in both early (PD, 1.51 (0.32); control, 2.26 (0.19); $p < 0.0001$) and delayed images (PD, 1.39 (0.33); control, 2.19 (0.20); $p < 0.0001$).

The age at examination was correlated with *H/M* ratio in patients with PD (early, $r = -0.42$, $p < 0.001$; delayed, $r = -0.44$, $p < 0.001$; fig 1), while in control subjects this age dependent reduction was not observed ($p > 0.5$). The age at onset was mildly but significantly negatively correlated with *H/M* ratio in PD (early, $r = -0.33$, $p = 0.002$; delayed,

Table 1 Ratio of ^{123}I-metaiodobenzylguanidine uptake in the heart to that in the mediastinum in four subgroups of patients with Parkinson's disease and in healthy control subjects

	Early image		Delayed image	
Patient subgroup	Median	Range	Median	Range
Older/severe	1.30* **	1.10-1.76	1.17* **	0.90-1.76
Older/mild	1.40**	1.12-2.60	1.27**	1.03-1.93
Younger/severe	1.50**	1.16-2.22	1.31**	1.17-2.49
Younger/mild	1.63* **	1.27-2.45	1.42* **	1.09-2.34
Controls	2.26	1.92-2.77	2.19	1.93-2.55

*p < 0.005; **p < 0.0001 compared with controls.

$r = -0.34$, $p = 0.001$; fig 2), and the H-Y scale was mildly but significantly correlated with *H/M* ratio (early, $r = -0.30$, $p = 0.006$; delayed, $r = -0.32$, $p = 0.003$; fig 3). The disease duration was not, however, significantly correlated with *H/M* ratio (early, $r = -0.15$, $p = 0.16$; delayed, $r = -0.20$, $p = 0.07$).

When the patients with PD were classified into the four groups on the basis of age at onset and disease severity, the median *H/M* ratios of each of these groups were significantly reduced as compared with controls ($p < 0.001$; table 1). The *H/M* ratio was lowest in the older/severe group in both early and delayed images of the four groups. The difference in *H/M* ratio between the older/severe group and younger/mild group was significant ($p < 0.005$; table 1).

DISCUSSION

Age at onset and H-Y scale are negatively correlated with both early and delayed cardiac MIBG uptake as assessed by the *H/M* ratio. Furthermore, the combination of higher age at onset and advanced H-Y stage profoundly influenced the reduction of myocardial MIBG uptake in PD. On the other hand, the disease duration was not significantly correlated with either early or delayed MIBG uptake. Both the age at examination and age at onset were negatively correlated with the *H/M* ratio. The age at examination includes the age at onset and the disease duration, so age at onset has a greater influence on the *H/M* ratio.

Several possible explanations for the pathophysiology underlying low myocardial MIBG uptake in PD have been proposed. Whether myocardial MIBG uptake reflects sympathetic and systemic autonomic failure has not been verified, and the degree of *H/M* ratio reduction is not always associated with the presence of orthostatic hypotension conditions.[11 15 17] We, however, have previously shown that patients with PD with orthostatic hypotension display supersensitivity to noradrenaline[21] and severely decreased MIBG uptake of not only the myocardium but also the lower extremities.[7] Recently, Goldstein *et al* showed that patients with PD with orthostatic hypotension had much lower cardiac uptake of 6-[18F] fluorodopamine than those without the condition.[22] Furthermore, they showed that lower 6-[18F] fluorodopamine was seen not only in the myocardium but also in the thyroid and renal cortex in PD with orthostatic hypotension, although we did not measure MIBG uptake in these organs in this study. These findings suggest that the sympathetic nerves are involved more extensively in PD than previously believed. As a possible explanation for the discrepancy between the reduction of myocardial MIBG uptake and orthostatic hypotension in PD, myocardial sympathetic nerve dysfunction would precede generalised sympathetic denervation eliciting orthostatic hypotension. On the other hand, pathological studies have shown that Lewy bodies and Lewy neurites are commonly identified in the cardiac plexus in PD,[23] and tyrosine hydroxylase immunoreactive nerve fibres in the heart are greatly decreased in patients with orthostatic hypotension.[24] Taken together, the degree of decreased myocardial MIBG uptake is thought to reflect the severity of myocardial sympathetic involvement and to be correlated with systemic sympathetic nerve involvement in PD.

In this study, cardiac MIBG uptake was mildly but significantly correlated with age at onset in PD. In control subjects, however, there were no significant differences in cardiac MIBG uptake in terms of aging. This was in agreement with a previous study by Tsuchimochi *et al*,[25] who reported reduced MIBG uptake in the inferior regions in older patients but no significant decrease in the whole myocardium. They proposed that sympathetic neuronal function in the inferior region may be selectively disturbed with aging. However, we found that sympathetic neuronal function disturbance was more extensively associated with the age at onset of PD. Thus, the negative correlation between age at onset and whole myocardial MIBG uptake was specifically associated with PD, but not with normal aging. Patients with a later onset of PD may have increased motor disability associated with more extensive subcortical involvement.[26 27] Furthermore, the degree of dementia caused by the presence of Lewy bodies in cortical areas has been shown to be related to the age at onset.[28 29] These reports indicate that a later onset may be associated with widespread multisystem involvement in PD.

We found that cardiac MIBG uptake had a mild but significant negative correlation with H-Y stage. Furthermore, cardiac MIBG uptake was significantly reduced in patients with PD with an H-Y score > III compared with those with an H-Y score ≤ II. In general, autonomic dysfunction in PD becomes apparent as the disease progresses.[30] Our findings indicate that the cardiac sympathetic nerve may be involved in the advancing severity of motor impairment in PD.

Patients with PD often have combinations of motor impairment, cognitive disorder, and autonomic failure during the course of the illness. However, the temporal progression of these three symptoms is heterogeneous among patients. Various factors have been proposed to influence the progression of PD. The present results suggest that patients with PD who have a combination of later onset and more severe clinical stage have increasing cardiac sympathetic nerve impairment in PD. Levy *et al*[31] reported that the increase in risk of dementia in PD was associated primarily with the combined effects of age and the severity of extrapyramidal signs.[31] Our findings are similar to those of Levy *et al* and suggest that later onset PD with high severity comes with an increased risk of early evolution not only to motor and cognitive system involvement but also to myocardial sympathetic involvement.

PD varies between patients in several respects, including age at onset and the rates of progression of both the severity of motor impairment and the involvement of multiple systems. Understanding the progression pattern of PD would provide novel targets for curative treatments on the basis of molecular and environmental studies. However, further prospective studies are needed to determine why age at onset and the severity of motor impairment are associated with reduced myocardial MIBG uptake in PD.

Authors' affiliations
K Hamada, M Hirayama, H Watanabe, R Kobayashi, H Ito, G Sobue, Department of Neurology, Nagoya University Graduate School of Medicine, Nagoya, Japan
T Ieda, Department of Neurology, Yokkaichi Municipal Hospital, Yokkaichi, Japan
Y Koike, Department of Medical Technology, Nagoya University School of Health Sciences, Nagoya, Japan

REFERENCES

1 **Wieland DM,** Wu JL, Brown LE, *et al.* Radiochemistry and radiopharmaceuticals: radiolabeled adrenergic neuron-blocking agents: adrenomedullary imaging with I-131 iodobenzylguanidine. *J Nucl Med* 1980;21:349–53.
2 **Stanton MS,** Tuli MM, Radike NL, *et al.* Regional sympathetic denervation after myocardial infarction in humans detected noninvasively using I-123 metaiodobenzylguanidine. *J Am Coll Cardiol* 1989;14:1519–26.
3 **Mantyasaari M,** Kuikka J, Mustonen J, *et al.* Noninvasive detection of cardiac sympathetic nervous dysfunction in diabetic patients using 123I-metaiodobenzylguanidine. *Diabetes* 1992;41:1069–75.
4 **Watanabe H,** Ieda T, Katayama T, *et al.* Cardiac ^{123}I-meta-iodobenzylguanidine (MIBG) uptake in dementia with Lewy bodies: comparison with Alzheimer's disease. *J Neurol Neurosurg Psychiatry* 2001;70:781–3.
5 **Watanabe H,** Misu K, Hirayama M, *et al.* Low cardiac ^{123}I-MIBG uptake in late-onset familial amyloid polyneuropathy type I (TTR Met30). *J Neurol* 2001;248:627–9.
6 **Hakusui S,** Yasuda T, Yanagi T, *et al.* A radiological analysis of heart sympathetic functions with meta-[123I]iodobenzylguanidine in neurological patients with autonomic failure. *J Auton Nerv Syst* 1994;49:81–4.
7 **Hirayama M,** Hakusui S, Koike Y, *et al.* A scintigraphical qualitative analysis of peripheral vascular sympathetic function with meta-[123I]iodobenzylguanidine in neurological patients with autonomic failure. *J Auton Nerv Syst* 1995;53:230–4.
8 **Yoshita M,** Hayashi M, Hirai S. Decreased myocardial accumulation of 123I-meta-iodobenzyl guanidine in Parkinson's disease. *Nucl Med Commun* 1998;19:137–42.
9 **Yoshita M.** Differentiation of idiopathic Parkinson's disease from striatonigral degeneration and progressive supranuclear palsy using iodine-123 meta-iodobenzylguanidine myocardial scintigraphy. *J Neurol Sci* 1998;155:60–7.
10 **Iwasa K,** Nakajima K, Yoshikawa H, *et al.* Decreased myocardial 123I-MIBG uptake in Parkinson's disease. *Acta Neurol Scand* 1998;97:303–6.
11 **Braune S,** Reinhardt M, Bathmann J, *et al.* Impaired cardiac uptake of meta-[123I]iodobenzylguanidine in Parkinson's disease with autonomic failure. *Acta Neurol Scand* 1998;97:307–14.
12 **Satoh A,** Serita T, Seto M, *et al.* Loss of 123I-MIBG uptake by the heart in Parkinson's disease: assessment of cardiac sympathetic denervation and diagnostic value. *J Nucl Med* 1999;40:371–5.
13 **Orimo S,** Ozawa E, Nakade S, *et al.* ^{123}I-metaiodobenzylguanidine myocardial scintigraphy in Parkinson's disease. *J Neurol Neurosurg Psychiatry* 1999;67:189–94.
14 **Braune S,** Reinhardt M, Schnitzer R, *et al.* Cardiac uptake of [123I]MIBG separates Parkinson's disease from multiple system atrophy. *Neurology* 1999;53:1020–5.
15 **Takatsu H,** Nishida H, Matsuo H, *et al.* Cardiac sympathetic denervation from the early stage of Parkinson's disease: clinical and experimental studies with radiolabeled MIBG. *J Nucl Med* 2000;41:71–7.
16 **Druschky A,** Hilz MJ, Platsch G, *et al.* Differentiation of Parkinson's disease and multiple system atrophy in early disease stages by means of I-123-MIBG-SPECT. *J Neurol Sci* 2000;175:3–12.
17 **Taki J,** Nakajima K, Hwang EH, *et al.* Peripheral sympathetic dysfunction in patients with Parkinson's disease without autonomic failure is heart selective and disease specific. *Eur J Nucl Med* 2000;27:566–73.
18 **Daniel SE,** Less AJ. Parkinson's Disease Society Brain Bank, London: overview and research. *J Neural Transm Suppl* 1993;39:165–72.
19 **Oliveri RL,** Zappia M, Annesi G, *et al.* The parkin gene is not involved in late-onset Parkinson's disease. *Neurology* 2001;57:359–62.
20 **Levy G,** Tang MX, Cote LJ, *et al.* Motor impairment in PD: relationship to incident dementia and age. *Neurology* 2000;55:539–44.
21 **Niimi Y,** Ieda T, Hirayama M, *et al.* Clinical and physiological characteristics of autonomic failure with Parkinson's disease. *Clin Auton Res* 1999;9:139–44.
22 **Goldstein DS,** Holmes CS, Dendi R, *et al.* Orthostatic hypotension from sympathetic denervation in Parkinson's disease. *Neurology* 2002;58:1247–55.
23 **Iwanaga K,** Wakabayashi K, Yoshimoto M, *et al.* Lewy body-type degeneration in cardiac plexus in Parkinson's and incidental Lewy body diseases. *Neurology* 1999;52:1269–71.
24 **Orimo S,** Ozawa E, Oka T, *et al.* Different histopathology accounting for a decrease in myocardial MIBG uptake in PD and MSA. *Neurology* 2001;57:1140–1.
25 **Tsuchimochi S,** Tamaki N, Tadamura E, *et al.* Age and gender differences in normal myocardial adrenergic neuronal function evaluated by iodine-123-MIBG imaging. *J Nucl Med* 1995;36:969–74.
26 **Granerus AK,** Carlsson A, Svanborg A, *et al.* The aging neuron influence on symptomatology and therapeutic response in Parkinson's syndrome. *Adv Neurol* 1979;24:327–34.
27 **Blin J,** Dubois B, Bonnet AM, *et al.* Does aging aggravate parkinsonian disability? *J Neurol Neurosurg Psychiatry* 1991;54:780–2.
28 **Hurtig HI,** Trojanowski JQ, Galvin J, *et al.* Alpha-synuclein-cortical Lewy bodies correlate with dementia in Parkinson's disease. *Neurology* 2000;54:1916–21.
29 **Apaydin H,** Ahlskog JE, Parisi JE, *et al.* Parkinson's disease neuropathology. Later-developing dementia and loss of the levodopa response. *Arch Neurol* 2002;59:102–12.
30 **Koike Y,** Takahashi A. Autonomic dysfunction in Parkinson's disease. *Eur Neurol* 1997;38(suppl 2):8–12.
31 **Levy G,** Schupf N, Tang MX, *et al.* Combined effect of age an severity on the risk of dementia in Parkinson's disease. *Ann Neurol* 2002;51:722–9.

BMJ Publishing Group
BMA House, Tavistock Square, London WC1H 9JR. Tel. 020 7383 6305. Fax 020 7383 6699

Printed in Great Britain by Meridian Print Centre Ltd. Derby. JNNP/Apr/03

Heat Shock Protein 70 Chaperone Overexpression Ameliorates Phenotypes of the Spinal and Bulbar Muscular Atrophy Transgenic Mouse Model by Reducing Nuclear-Localized Mutant Androgen Receptor Protein

Hiroaki Adachi,[1] Masahisa Katsuno,[1] Makoto Minamiyama,[1] Chen Sang,[1] Gerassimos Pagoulatos,[2] Charalampos Angelidis,[2] Moriaki Kusakabe,[3] Atsushi Yoshiki,[4] Yasushi Kobayashi,[1] Manabu Doyu,[1] and Gen Sobue[1]

[1]Department of Neurology, Nagoya University Graduate School of Medicine, 65 Tsurumai-cho Showa-ku, Nagoya 466-8550, Japan, [2]Department of General Biology, University of Ioannina, School of Medicine, Ioannina GR-45110, Greece, [3]ANB Tsukuba Institute, ALOKA Company, Ltd., 1103 Fukaya, Kasumigaura, Niihari, Ibaraki 300-0134, Japan, and [4]Experimental Animal Division, Department of Biological Systems, BioResource Center, The Institute of Physical and Chemical Research (RIKEN) Tsukuba Institute 3-1-1 Koyadai, Tsukuba, Ibaraki 305-0074, Japan

Spinal and bulbar muscular atrophy (SBMA) is an inherited motor neuron disease caused by the expansion of the polyglutamine (polyQ) tract within the androgen receptor (AR). The nuclear inclusions consisting of the mutant AR protein are characteristic and combine with many components of ubiquitin–proteasome and molecular chaperone pathways, raising the possibility that misfolding and altered degradation of mutant AR may be involved in the pathogenesis. We have reported that the overexpression of heat shock protein (HSP) chaperones reduces mutant AR aggregation and cell death in a neuronal cell model (Kobayashi et al., 2000). To determine whether increasing the expression level of chaperone improves the phenotype in a mouse model, we cross-bred SBMA transgenic mice with mice overexpressing the inducible form of human HSP70. We demonstrated that high expression of HSP70 markedly ameliorated the motor function of the SBMA model mice. In double-transgenic mice, the nuclear-localized mutant AR protein, particularly that of the large complex form, was significantly reduced. Monomeric mutant AR was also reduced in amount by HSP70 overexpression, suggesting the enhanced degradation of mutant AR. These findings suggest that HSP70 overexpression ameliorates SBMA phenotypes in mice by reducing nuclear-localized mutant AR, probably caused by enhanced mutant AR degradation. Our study may provide the basis for the development of an HSP70-related therapy for SBMA and other polyQ diseases.

Key words: **HSP70; chaperone; polyglutamine; SBMA; transgenic mice; protein degradation**

Introduction

Polyglutamine (polyQ) diseases are inherited neurodegenerative disorders caused by the expansion of a trinucleotide CAG repeat in the causative genes (Zoghbi and Orr, 2000). To date, nine polyQ diseases have been identified (Ross, 2002). Spinal and bulbar muscular atrophy (SBMA) is a polyQ disease, characterized by proximal muscle atrophy, weakness, contraction fasciculations, and bulbar involvement (Kennedy et al., 1968; Sobue et al., 1989; Takahashi, 2001). In SBMA, a polymorphic CAG repeat with 14–32 CAGs expands to 40–62 CAGs in the first exon of the androgen receptor (*AR*) gene (Tanaka et al., 1996) and has somatic mosaicism (Tanaka et al., 1999). There is an inverse correlation between the CAG repeat size and the age at onset or the disease severity in SBMA (Doyu et al., 1992; Igarashi et al., 1992; La Spada et al., 1992). In SBMA, nuclear inclusions (NIs) containing mutant AR have been observed in the brainstem motor nuclei, spinal motor neurons, and some visceral organs (Li et al., 1998a,b). Such neuronal inclusions are common pathological features in polyQ diseases and are also colocalized with many components of ubiquitin–proteasome and molecular chaperones (Chai et al., 1999; Huynh et al., 2000; Adachi et al., 2001; Zander et al., 2001; Schmidt et al., 2002), raising the possibility that misfolding and altered degradation of the mutant protein may be involved in the pathogenesis of SBMA as well as other polyQ diseases (Stenoien et al., 1999; Waelter et al., 2001). Furthermore, these chaperones and proteasomes would facilitate refolding or proteolysis of the mutant protein and may play a role in protecting neuronal cells against the toxic properties of the expanded polyQ (Cummings et al., 1998; Kobayashi et al., 2000). We have shown recently that overexpression of heat shock proteins (HSPs) decreases the aggregate formation of truncated AR with the expanded polyQ and markedly prevents cell death in the neuronal cell model of SBMA (Kobayashi et al., 2000; Kobayashi and Sobue, 2001). HSP70 overexpression has been reported to enhance the solubility and degradation of mutant AR (Bailey et al., 2002). HSPs have also been shown to suppress aggregate formation and cellular toxicity in a wide range of polyQ disease models (Cummings et al., 1998; Warrick et al., 1999; Carmichael et al., 2000). Recently, overexpression of the inducible form of rat

Received Nov. 5, 2002; revised Dec. 31, 2002; accepted Dec. 31, 2002.

This work was supported by a Center of Excellence grant from the Ministry of Education, Culture, Sports, Science, and Technology of Japan and by grants from the Ministry of Health, Labor, and Welfare of Japan. We thank Sugiko Yokoi for her technical assistance.

Correspondence should be addressed to Dr. Gen Sobue, Department of Neurology, Nagoya University Graduate School of Medicine, 65 Tsurumai-cho Showa-ku, Nagoya, 466-8550, Japan. E-mail: sobueg@med.nagoya-u.ac.jp.

 0270-6474/03/232203-09$15.00/0

HSP70 ameliorated neurologic deficits and the neuronal degeneration of spinocerebellar ataxia type 1 (SCA1) transgenic mice, whereas the NIs consisting of mutant ataxin-1 were not reduced (Cummings et al., 2001).

In the present study, we report that overexpression of the inducible form of human HSP70 markedly ameliorated clinical and pathological phenotypes, and that this amelioration was correlated with the reduction of nuclear-localized mutant AR protein complexes in the mouse model of SBMA (Katsuno et al., 2002). Furthermore, the amount of monomeric mutant AR was also significantly reduced in the double-transgenic mice, suggesting that the degradation of mutant AR may have been accelerated by the overexpression of HSP70.

Materials and Methods

Assessment of motor ability. All animal experiments were performed in accordance with the National Institutes of Health *Guide for the Care and Use of Laboratory Animals* and were approved by the Nagoya University Animal Experiment Committee. Motor ability was assessed using an Economex Rotarod (Columbus Instruments, Columbus, OH) on a weekly basis as described previously (Adachi et al., 2001). The period for which a mouse could remain on a rotating axle (diameter, 3.6 cm; speed of rotation, 16 rpm) without falling was measured. Three trials were performed, and the longest duration on the rod was recorded for every mouse. The timer was stopped if the mouse fell from the rod or after an arbitrary limit of 180 sec. Cage activity was measured weekly while each mouse was in a transparent acrylic cage (16 × 30 × 14 cm, width × depth × height) within a soundproofed box as described previously (Katsuno et al., 2002). Spontaneous motor activity was measured by means of an animal behavior system (Neuroscience Inc., Tokyo, Japan), which monitored and counted all spontaneous movements, both vertical and horizontal, including locomotion, rearing, head movements, etc. All counts were automatically totaled and recorded in 24 hr.

Immunohistochemistry. We perfused 20 ml of a 4% paraformaldehyde fixative in 0.1 M phosphate buffer, pH 7.4, through the left cardiac ventricle of mice deeply anesthetized with ketamine–xylazine, postfixed tissues in 10% phosphate-buffered formalin, and processed tissues for paraffin embedding. Then we deparaffinized 4-μm-thick tissue sections, dehydrated with alcohol, and treated for antigen retrieval (Katsuno et al., 2002). For the HSP70 immunohistochemical study, the paraffin sections were pretreated with trypsin (Dako, Glostrup, Denmark) for 20 min at 37°C. The tissue sections were blocked with normal animal serum (1:20) and incubated with mouse anti-expanded polyQ (1:10,000) (1C2; Chemicon, Temecula, CA) and goat polyclonal antibody to HSP70 (1:500) (K-20; Santa Cruz Biotechnology, Santa Cruz, CA). Then the sections were incubated with biotinylated anti-species-specific IgG (Vector Laboratories, Burlingame, CA). Immune complexes were visualized using streptavidin–horseradish peroxidase (Dako) and 3,3′-diaminobenzidine (Dojindo, Kumamoto, Japan) substrate. Sections were counterstained with methyl green.

For double-labeling immunohistochemistry, sections were preincubated with normal horse serum diluted in 0.02 M PBS buffer, pH 7.4, containing bovine serum albumin. The sections were then incubated with goat anti-HSP70 antibody (1:500) (K-20; Santa Cruz) at 4°C overnight, washed with 0.02 M PBS buffer, incubated with biotinylated horse anti-goat IgG, stained with streptavidin–alkaline phosphatase, and visualized with fast red. 1C2 antibody (1:10,000; Chemicon) was subsequently applied to sections at 4°C overnight. After being washed, the sections were incubated with horseradish peroxidase-labeled donkey anti-mouse Ig $F(ab')_2$ (Amersham Biosciences, Buckinghamshire, UK), which had been demonstrated to cross-react with neither goat nor horse sera, and visualized with 3,3′-diaminobenzidine. For double-immunofluorescence staining of the spinal cord, sections were blocked with 5% normal horse serum and then sequentially incubated with K-20 antibody (1:500; Santa Cruz Biotechnology) and 1C2 antibody (1:10,000; Chemicon) at 4°C overnight. After incubation with biotinylated horse anti-goat IgG (Vector Laboratories) for 8 hr at 4°C, the sections were incubated with Alexa-488-conjugated streptavidin (1:400; Molecular Probes, Leiden, The Netherlands) and Alexa-568-conjugated goat anti-mouse IgG (1:1300; Molecular Probes), which had been demonstrated to cross-react with neither goat nor horse sera, for 8 hr at 4°C. The sections were then examined and photographed under a confocal laser scanning microscope (MRC 1024; Bio-Rad, Hercules, CA).

As for the immunohistochemistry of SBMA patients, nine patients with clinicopathologically and genetically confirmed SBMA (age, 51–84 years; mean, 64.3) and three non-neurological controls (age, 51–76 years; mean, 64.0) served as the subjects of the present study. Paraffin-embedded sections of the spinal cord and brain were obtained and examined in the same way as for the transgenic mice.

Quantification of 1C2-positive cells in the spinal cord and muscle. For the assessment of 1C2-positive cells, 4-μm-thick coronal sections of the thoracic spinal cord and gastrocnemius muscle stained by 1C2 antibody (1:10,000; Chemicon) were prepared, and the number of 1C2-positive cells for one mouse was counted using a light microscope with a computer-assisted image analyzer (Luzex FS; Nikon, Tokyo, Japan). For the assessment of 1C2-positive cells in the ventral horn of the spinal cord, 50 consecutive transverse sections of the thoracic spinal cord were prepared, and the 1C2-positive cells present within the ventral horn on every fifth section were counted as described previously (Terao et al., 1996; Adachi et al., 2001). Populations of 1C2-positive cells were expressed as the number per square millimeter. For the assessment of 1C2-positive cells in the muscle, 1C2-positive cells were calculated from counts of >500 fibers in randomly selected areas and were expressed as the number per 100 muscle fibers.

Western blots. We exsanguinated mice under ketamine–xylazine anesthesia and snap-froze their tissues with powdered CO_2 in acetone. Frozen tissue (0.1 gm wet weight) was homogenized in 1000 μl of lysis buffer (50 mM Tris-HCl, pH 8.0, 150 mM NaCl, 1% NP-40, 0.5% deoxycholate, and 0.1% SDS with 1 mM PMSF and aprotinin at 6 μg/ml). Homogenates were spun at 2500 × *g* for 15 min at 4°C. The protein concentration of the supernatant was determined using detergent-compatible protein assay (Bio-Rad). Each lane on a 5–20% SDS-PAGE gel was loaded with protein (200 μg for the spinal cord and 80 μg for the muscle from the supernatant fraction), which was transferred to Hybond-P membranes (Amersham Biosciences) using 25 mM Tris, 192 mM glycine, 0.1% SDS, and 10% methanol as transfer buffer. Kaleidoscope prestained standards were used as size markers (Bio-Rad). Proteins were then transferred to Hybond-P membranes, which were subsequently blocked in 5% milk in TBS containing 0.05% Tween 20 and incubated with appropriate primary antibodies using standard techniques. Primary antibodies were used at the following concentrations: rabbit anti-AR antibody (1:1000 N-20; Santa Cruz Biotechnology); mouse anti-HSP70/heat shock cognate 70 (HSC70) antibody (1:5000, W-27; Santa Cruz Biotechnology). We performed second antibody probing and detection using the ECL+plus kit (Amersham Biosciences). The HRP-conjugated secondary antibodies used were anti-rabbit Ig $F(ab')_2$ and anti-mouse Ig $F(ab')_2$ (1:5000; Amersham Biosciences). Nuclear and cytoplasmic fractions were extracted with a NE-PER Nuclear and Cytoplasmic Extraction Reagents Kit according to the protocol of the manufacturer (Pierce, Rockford, IL). Each lane on a 5–20% SDS-PAGE gel was loaded with 200 μg of protein for the spinal cord and 80 μg for the muscle from each fraction. Immunoprecipitation was performed using 1 mg of the total protein lysate, 10 μl of protein G–Sepharose (Amersham Biosciences), and 5 μl of anti-AR antibody (N-20; Santa Cruz Biotechnology). Protein was eluted from beads by boiling for 3 min in 10 μl of elution buffer (50 mM Tris-HCl, pH 6.8, 2% SDS, 60 μl/ml 2-mercaptoethanol, and 10% glycerol). The elutes were loaded on SDS–polyacrylamide gels. Blots were sequentially probed with goat anti-HSP70 antibody (K-20; Santa Cruz Biotechnology).

The signal intensity was analyzed using the NIH Image program (version 1.62). Relative signal intensity was computed as the signal intensity of each sample divided by that of the AR-97Q/HSP70$^{(-/-)}$ mice.

Filter-trap assay. Filtration of proteins through a 0.2 μm cellulose acetate membrane (Sartorius AG, Goettingen, Germany) was performed using a slot-blot apparatus (Bio-Rad). The membranes were washed

three times with TBS buffer and supported by three pieces of filter paper (Bio-Rad). We also put 0.45 μm nitrocellulose membrane (Bio-Rad) under the cellulose acetate membrane to capture the monomeric AR protein passing through this membrane. Samples of protein (200 μg) for the spinal cord and for the muscle (80 μg) were prepared in a final volume of 200 μl in lysis buffer, loaded, and gently vacuumed. Membranes were washed three times with TBS containing 0.05% Tween 20. Slot-blots were probed as described for Western blots.

Statistical analysis. We analyzed data using the unpaired *t* test and log-rank test from Statview software version 5 (Hulinks, Tokyo, Japan).

Results

Nondeleterious effects of HSP70 overexpression and generation of double-transgenic mice

Because HSP70s have a wide variety of functions, we examined whether the overexpression of HSP70 under the control of the human β-actin promoter has deleterious effects on phenotypes in mice (Plumier et al., 1995). Motor function in the mice with HSP70 overexpression was not affected; a Rotarod task until 40 weeks revealed no impairment in either hemizygous or homozygous transgenic mice overexpressing HSP70 (data not shown). Histological examination at 40 weeks of age did not show any detectable effect on the neuronal cell morphology and population and on the muscular structure in the overexpression of human HSP70 alone (data not shown). These studies indicated that the overexpression of human HSP70 alone does not impair neuronal development and motor function.

To determine whether the overexpression of human HSP70 could ameliorate the disease phenotype of the SBMA transgenic mouse model, we crossed the mice expressing full-length human AR with 97-polyQ tract (AR-97Q mice, 4–6 line) (Katsuno et al., 2002) with mice that overexpress human HSP70 under the control of the human β-actin promoter (Plumier et al., 1995). The SBMA model (AR-97Q mice) shows small body size, short lifespan, progressive muscle atrophy and weakness, and reduced cage activity (Katsuno et al., 2002). Because the phenotypes of these SBMA transgenic mice are markedly pronounced in male transgenic mice similarly to SBMA patients (Katsuno et al., 2002), we used male transgenic mice in this study. We generated the AR-97Q/HSP70$^{(tg/tg)}$ mice as homozygotes and the AR-97Q/HSP70$^{(tg/-)}$ mice as hemizygotes, as well as the AR-97Q/HSP70$^{(-/-)}$ mice as a control transgenic mouse line. The SBMA transgene expression was at the hemizygous level in all AR-97Q/HSP70 double-transgenics.

Human HSP70 overexpression ameliorates motor phenotypes of SBMA transgenic mice

To determine whether HSP70 overexpression has an ameliorative effect on the motor phenotypes, we performed the Rotarod task and the measurement of locomotor cage activity by infrared sensor system with the double-transgenic mice (Fig. 1*A*,*B*). The AR-97Q/HSP70$^{(-/-)}$ mice showed motor impairment on the Rotarod task as early as 9 weeks after birth; by 12 weeks and 25 weeks of age they began to show significant impairment compared with AR-97Q/HSP70$^{(tg/-)}$ mice ($p < 0.05$) and AR-97QHSP70$^{(tg/tg)}$ mice ($p < 0.001$), respectively. (Fig. 1*A*). Although both the AR-97Q/HSP70$^{(tg/tg)}$ and AR-97Q/HSP70$^{(tg/-)}$ mice performed better than the AR-97Q/HSP70$^{(-/-)}$ mice, the AR-97Q/HSP70$^{(tg/tg)}$ mice were on the rod longer than the AR-97Q/HSP70$^{(tg/-)}$ mice during the trial. The locomotor cage activity of the AR-97Q/HSP70$^{(-/-)}$ mice was also significantly decreased at 21 weeks in comparison with the other two double-transgenics ($p < 0.05$) (Fig. 1*B*). No lines were distinguishable in terms of body weight at birth. The AR-97Q/HSP70$^{(-/-)}$ mice lost

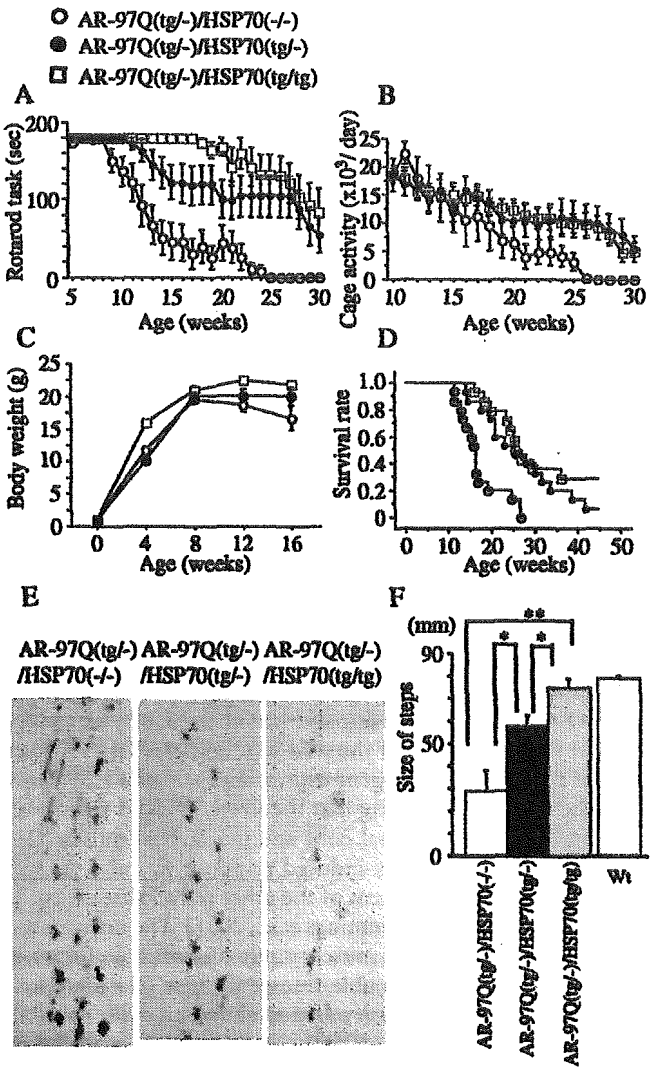

Figure 1. Effects of human HSP70 overexpression on the symptomatic phenotypes of male AR-97Q mice. Rotarod task (*A*; $n = 10$), cage activity (*B*; $n = 10$), body weight (*C*; $n = 12$), and survival rate (*D*; $n = 14$) of the AR-97Q/HSP70$^{(-/-)}$, AR-97Q/HSP70$^{(tg/-)}$, and AR-97Q/HSP70$^{(tg/tg)}$ mice. All parameters were significantly different among AR-97Q/HSP70$^{(-/-)}$ mice, AR-97Q/HSP70$^{(tg/tg)}$, and AR-97Q/HSP70$^{(tg/-)}$ mice ($p < 0.001$, $p < 0.05$, $p < 0.05$, and $p < 0.005$, respectively). AR-97Q mice overexpressing human HSP70 lasted longer on the Rotarod and showed higher cage activity than AR-97Q/HSP70$^{(-/-)}$ mice. The AR-97Q/HSP70$^{(-/-)}$ mice lost weight earlier than the other two double-transgenics. Survival was prolonged in AR-97Q/HSP70$^{(tg/-)}$ and AR-97Q/HSP70$^{(tg/tg)}$ mice compared with AR-97Q/HSP70$^{(-/-)}$ mice. *E*, Footprints of representative 16-week-old AR-97Q/HSP70$^{(-/-)}$, AR-97Q/HSP70$^{(tg/-)}$, and AR-97Q/HSP70$^{(tg/tg)}$ mice. Front paws are indicated in *red* and hindpaws in *blue*. AR-97Q/HSP70$^{(-/-)}$ mice exhibit motor weakness, with dragging of the legs; AR-97Q/HSP70$^{(tg/tg)}$ mice walk almost normally; and AR-97Q/HSP70$^{(tg/-)}$ mice walk with somewhat short steps. *F*, The size of steps was measured in 16-week-old AR-97Q/HSP70$^{(-/-)}$, AR-97Q/HSP70$^{(tg/-)}$, and AR-97Q/HSP70$^{(tg/tg)}$ mice ($n = 4$), respectively. Each column shows an average of steps of the hindpaw. AR-97Q/HSP70$^{(tg/-)}$ and AR-97Q/HSP70$^{(tg/tg)}$ mice walked with significantly longer steps than AR-97Q/HSP70$^{(-/-)}$ mice. *$p < 0.05$; **$p < 0.01$. Error bars indicate SD. *Wt*, Wild type.

weight significantly earlier than the AR-97Q/HSP70$^{(tg/tg)}$ mice ($p < 0.01$) (Fig. 1*C*). The survival rate was significantly more prolonged in the AR-97Q/HSP70$^{(tg/-)}$ and AR-97Q/HSP70$^{(tg/tg)}$ mice than in the AR-97Q/HSP70$^{(-/-)}$ mice ($p < 0.01$ and $p < 0.005$, respectively) (Fig. 1*D*). The affected AR-97Q/HSP70$^{(-/-)}$ mice exhibited motor weakness, with dragging of the legs or short steps, whereas the AR-97Q/HSP70$^{(tg/tg)}$ mice showed almost normal ambulation and the AR-97Q/HSP70$^{(tg/-)}$ mice only

somewhat short steps (Fig. 1*E*). The AR-97Q/HSP70$^{(tg/-)}$ and AR-97Q/HSP70$^{(tg/tg)}$ mice showed significantly longer steps than the AR-97Q/HSP70$^{(-/-)}$ mice (Fig. 1*F*). Although both the AR-97Q/HSP70$^{(tg/tg)}$ and AR-97Q/HSP70$^{(tg/-)}$ mice showed ameliorated phenotypic expressions, the AR-97Q/HSP70$^{(tg/tg)}$ mice were better than the AR-97Q/HSP70$^{(tg/-)}$ mice in most of the parameters, suggesting that the improved motor phenotype depended on the HSP70 expression level rather than on the genetic background.

Expression levels of HSP70 in double-transgenic mice

We examined whether the AR-97Q/HSP70 double-transgenic mice express increased levels of the HSP70 protein in the spinal cord and skeletal muscle. Immunohistochemical studies of double-transgenic mice stained with the specific antibody for HSP70 confirmed that spinal neurons and muscular cells expressed the HSP70 (Fig. 2*A–C*). The HSP70 was diffusely distributed to the nuclei and occasionally formed various-sized NIs (Fig. 2*A–C*). Glial cells also showed diffuse nuclear staining and NIs of HSP70 protein (data not shown). Western blot analysis revealed that the HSP70 expression level was fivefold greater in the AR-97Q/HSP70$^{(tg/-)}$ mice and 10-fold greater in the AR-97Q/HSP70$^{(tg/tg)}$ mice than endogenous HSP70 in the AR-97Q/HSP70$^{(-/-)}$ mice in the spinal cord and muscle (Fig. 2*D*). The AR-97Q transgene expression did not alter HSP70 expression levels in the spinal cord of the wild-type and HSP70$^{(tg/tg)}$ mice, whereas the AR-97Q transgene expression increased HSP70 levels in the muscle, suggesting that the stress-induced response is different between the spinal cord and the skeletal muscle (Fig. 2*D*). Absence of the stress-induced response was also demonstrated in the nervous system of the other polyQ disease model mice (Jana et al., 2000; Cummings et al., 2001). The nuclear fraction of the spinal cord and muscle surely contained an increased amount of HSP70 in the double-transgenic mice. The amount of HSP70 in the nuclear fraction was most abundant in the AR-97Q/HSP70$^{(tg/tg)}$ mice (Fig. 2*E*). The increased HSP70 was coimmunoprecipitated with mutant AR, suggesting that HSP70 directly binds to the mutant AR protein (Fig. 2*F*).

Colocalization of HSP70 with mutant AR in the nuclei

We evaluated the colocalization of HSP70 and mutant AR in the AR-97Q/HSP70 double-transgenic mice. We performed double-labeling immunohistochemistry and immunofluorescence double-staining with two primary antibodies: goat anti-HSP70 and mouse anti-expanded polyQ (1C2). These double-immunostaining studies revealed that HSP70 (Fig. 3*A,C*) and mutant AR (Fig. 3*B,D*) present diffusely in the nuclei and colocalize each other (Fig. 3*B,E*) in the spinal anterior horn neurons of the AR-97Q/HSP70$^{(tg/tg)}$ mice. We also determined that such diffuse staining of HSP70 in the nuclei was also present in the spinal neurons of SBMA patients (Fig. 3*F,I*). Immunofluorescence double-staining with anti-HSP70 and anti-expanded polyQ antibodies revealed that the endogenous HSP70 (Fig. 3*G,K*) and mutant AR (Fig. 3*H,L*) were colocalized on the NI (Fig. 3*I*) and diffusely in the nuclei (Fig. 3*M*) in the spinal cord neurons of SBMA patients, suggesting that the endogenous HSP70 preferentially coexists with mutant AR and exerts its function in the nuclei of SBMA patients as well.

Overexpression of HSP70 decreases the nuclear-localized mutant AR

An immunohistochemical study for mutant AR using 1C2 antibody showed a marked reduction in diffuse nuclear staining and NIs in the AR-97Q/HSP70$^{(tg/-)}$ or the AR-97Q/HSP70$^{(tg/tg)}$ mice compared with the AR-97Q/HSP70$^{(-/-)}$ mice in the spinal motor neurons (Fig. 4*A–C*) and muscles (Fig. 4*D–F*). The AR-97Q/HSP70$^{(-/-)}$ mice showed intense and frequent 1C2 staining in the nuclei (Fig. 4*A,D*), whereas the 1C2 staining was infrequent

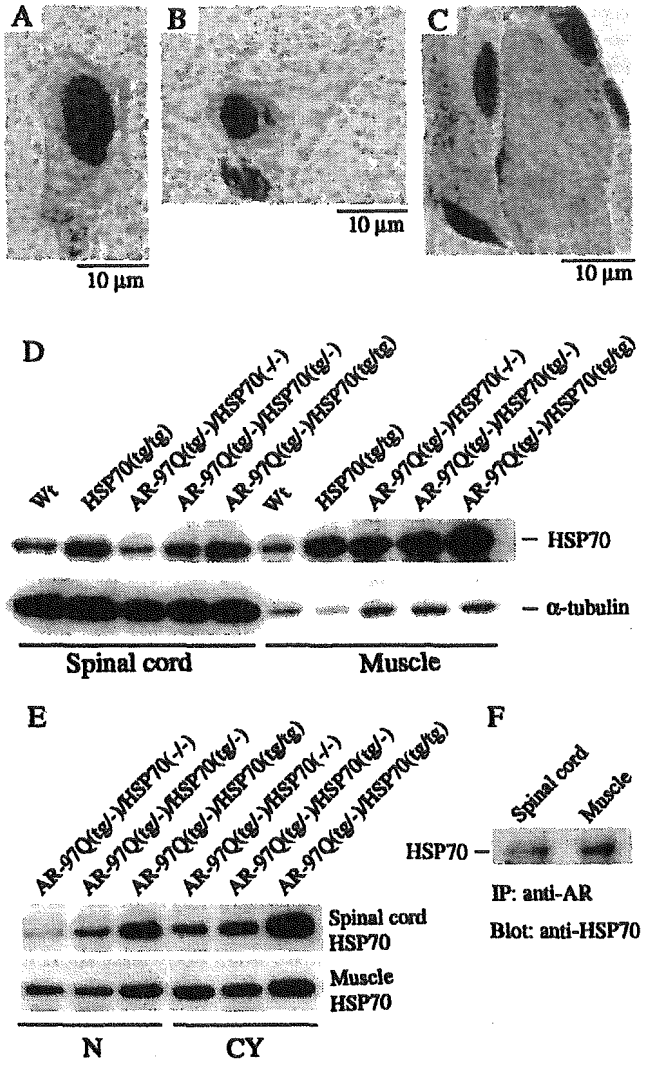

Figure 2. Increased HSP70 expression in double-transgenic mice. *A–C*, Immunohistochemical study from the 16-week-old AR-97Q/HSP70$^{(tg/-)}$ mice in the spinal anterior horn and skeletal muscle stained with the antibody specific for the HSP70. The immunoreactivity of HSP70 was localized to the nuclei with intense and diffuse staining, and small NIs were present in the anterior horn cell (*A*). A large nuclear inclusion was also present in the anterior horn cell (*B*). Skeletal muscle showed diffuse nuclear staining and NIs (*C*). *D, E*, Western blot analysis of total spinal cord and muscle protein lysate immunolabeled with an antibody against HSP70. AR-97Q/HSP70$^{(tg/-)}$ and AR-97Q/HSP70$^{(tg/tg)}$ mice express higher levels of HSP70 than wild-type (*Wt*) and AR-97Q/HSP70$^{(-/-)}$ mice (*D*). The HSP70 expression level is fivefold higher in AR-97Q/HSP70$^{(tg/-)}$ mice and 10-fold higher in the AR-97Q/HSP70$^{(tg/tg)}$ mice than endogenous HSP70 in AR-97Q/HSP70$^{(-/-)}$ mice in the spinal cord and muscle, respectively (*D*). The AR-97Q transgene expression did not alter HSP70 levels in the spinal cord, whereas the AR-97Q transgene expression gained the respective HSP70 levels in the muscle (*D, E*). Therefore, the AR-97Q transgene expression in the double-transgenics alters HSP70 levels in the muscle but not in the spinal cord. *E*, Western blots of nuclear and cytoplasmic extracts immunolabeled with an antibody against HSP70. HSP70 localized in the nucleus (*N*) as well as in the cytoplasm (*CY*) in the spinal cord and muscle of all lines examined. AR-97Q/HSP70$^{(tg/tg)}$ mice expressed the largest amount of HSP70 in both extracts. *F*, Immunoprecipitation (*IP*) Western blots for HSP70. Soluble fractions were collected from the spinal cord and muscle, and equal protein concentrations were immunoprecipitated with an antibody to the N-terminal portion of AR and immunoblotted for HSP70. Coimmunoprecipitation of the HSP70 chaperone and the polyQ-expanded mutant AR was detected.

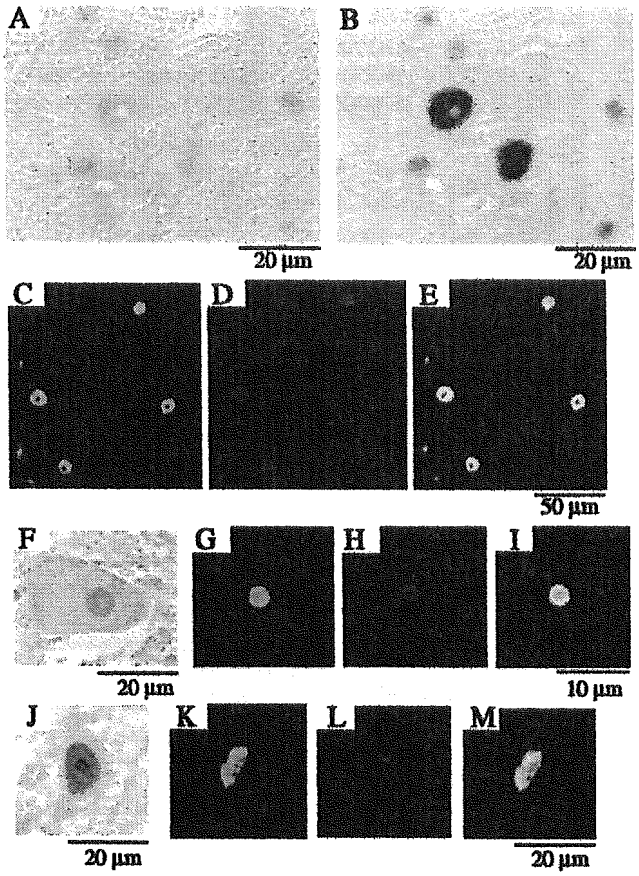

Figure 3. Colocalization of the nuclear-localized HSP70 chaperone with mutant AR. Immunohistochemical analysis for the antibody specific to the HSP70 as well as to the expanded polyQ stretch (immunostained with a monoclonal antibody, 1C2) in the spinal cords of 16-week-old AR-97Q/HSP70$^{(tg/tg)}$ mice (*A–E*) and SBMA patients (*F–M*). Double-labeling immunohistochemistry revealed diffuse nuclear staining for goat anti-HSP70 (*A*) and expanded polyQ (*B*), suggesting that HSP70 and mutant AR are colocalized in the spinal motor neurons of AR-97Q/HSP70$^{(tg/tg)}$ mice. Immunofluorescence double-staining with antibodies against HSP70 and the expanded polyQ also revealed that HSP70 and mutant AR are colocalized as shown in HSP70 (*C, green*), expanded-polyQ (*D, red*), and an overlay of the two signals (*E, yellow*). Diffuse staining of neuronal nuclei for HSP70 is also observed in the spinal neurons (*F, J*) of SBMA patients. Immunofluorescence double-staining with anti-HSP70 (*green*) and anti-expanded polyQ (*red*) antibodies revealed that the HSP70 (*G*) and mutant AR (*H*) are colocalized on the NI (shown in *yellow* in *I*) in the spinal anterior horn cell. The diffuse nuclear colocalization of HSP70 (*K*) and mutant AR (*H*) was also observed in the SBMA posterior horn cell (*M*). This cell also has an NI (*L, M*).

in the AR-97Q/HSP70$^{(tg/-)}$ mice (Fig. 4*B,E*) and much less frequent in the AR-97Q/HSP70$^{(tg/tg)}$ mice (Fig. 4*C,F*). Quantitative assessment of diffuse nuclear staining for 1C2 in the spinal motor neurons (Fig. 4*G*) and muscles (Fig. 4*H*) revealed significantly more positive cells in the AR-97Q/HSP70$^{(-/-)}$ mice than in the AR-97Q/HSP70$^{(tg/-)}$ and AR-97Q/HSP70$^{(tg/tg)}$ mice. However, the 1C2-positive cell populations were not statistically different in the AR-97Q/HSP70$^{(tg/-)}$ and the AR-97Q/HSP70$^{(tg/tg)}$ mice. The neuronal cell population in the spinal ventral horn in the AR-97Q/HSP70$^{(-/-)}$, AR-97Q/HSP70$^{(tg/-)}$, and AR-97Q/HSP70$^{(tg/tg)}$ mice was not significantly decreased compared with that in the wild-type mice (data not shown).

Overexpression of HSP70 decreases the high-molecular-weight mutant AR protein and monomeric mutant AR protein

Western blot analysis showed that the high-molecular-weight form of mutant AR protein complexes was retained in the stacking gel as well as a band of monomeric mutant AR monomer in the spinal cord and muscle of the transgenic mice (Fig. 5). The mutant AR within the stacking gel was diminished in the AR-97Q/HSP70$^{(tg/-)}$ and AR-97Q/HSP70$^{(tg/tg)}$ mice compared with the AR-97Q/HSP70$^{(-/-)}$ mice (Fig. 5*A,B*). In addition, the AR-97Q/HSP70$^{(-/-)}$ mice had more monomeric mutant AR protein than the AR-97Q/HSP70$^{(tg/-)}$ or AR-97Q/HSP70$^{(tg/tg)}$ mice (Fig. 5*A,B*). The mutant AR protein within the stacking gel was found primarily in the nuclear fraction (Fig. 5*C*). The mutant AR within the stacking gel and monomeric form of the nuclear fraction in the spinal cord and muscle were also decreased in the AR-97Q/HSP70$^{(tg/-)}$ and AR-97Q/HSP70$^{(tg/tg)}$ mice (Fig. 5*C*). These observations suggested that the overexpression of HSP70 markedly decreases not only the high-molecular-weight mutant AR protein present primarily in the nuclear fraction but also the monomeric mutant AR protein.

We next performed a filter-trap assay for the quantitative analysis of the large molecular aggregated and soluble monomeric form of the mutant AR protein (Wanker et al., 1999). Only the larger-sized mutant AR protein was retained on the cellulose acetate membrane (pore diameter, 0.2 μm), whereas the nitrocellulose membrane captured proteins of all sizes (Fig. 6*A*). We also put the nitrocellulose membrane under the cellulose acetate membrane to capture the soluble monomeric AR protein passing through this membrane (Fig. 6*B*). Values were normalized to endogenous α-tubulin using the nitrocellulose membrane. Using this approach, we analyzed the ability of the HSP70 to decrease the large aggregated or soluble monomeric mutant AR protein. Overexpression of HSP70 resulted in a significant decrease in large aggregated as well as soluble monomeric mutant AR protein in a dose-dependent manner (Fig. 6*A–C*). The endogenous AR protein was not retained on the cellulose acetate membrane in wild-type mice (data not shown). These results indicate that the HSP70 decreases not only the mutant AR protein complexes in the large aggregated form but also the soluble monomeric mutant AR as observed on Western blot analysis. These observations also suggested that overexpression of HSP70 enhanced the function of the ubiquitin–proteasome pathway and subsequently accelerated the degradation of monomeric mutant AR protein.

Discussion

We generated a transgenic mouse model carrying a full-length AR containing 97 CAGs (Katsuno et al., 2002). This model showed progressive muscular atrophy and weakness as well as diffuse nuclear staining and NIs consisting of the mutant AR. These phenotypes were very pronounced in male transgenic mice, similar to those in SBMA (Katsuno et al., 2002). Here we demonstrate that the overexpression of human HSP70 exerts dose-dependent therapeutic effects on motor dysfunction in this mouse model. Mutant AR and HSP70 colocalized diffusely to the nuclei and to the NIs in the neurons and muscles of the AR-97Q/HSP70 double-transgenic mice. The overexpression of HSP70 served to decrease the nuclear-localized mutant AR protein complexes in large aggregated form in the double-transgenic mice. Monomeric mutant AR was also significantly reduced by HSP70 overexpression, suggesting that it could accelerate the turnover of mutant AR.

In our SBMA transgenic mouse model, nuclear translocation of mutant AR, which is dependent on the testosterone level, has been demonstrated to be essential for mutant AR-induced neurotoxicity (Katsuno et al., 2002). Reduction of the testosterone level by castration diminished nuclear-localized mutant AR and markedly prevented phenotypic expression in the male trans-

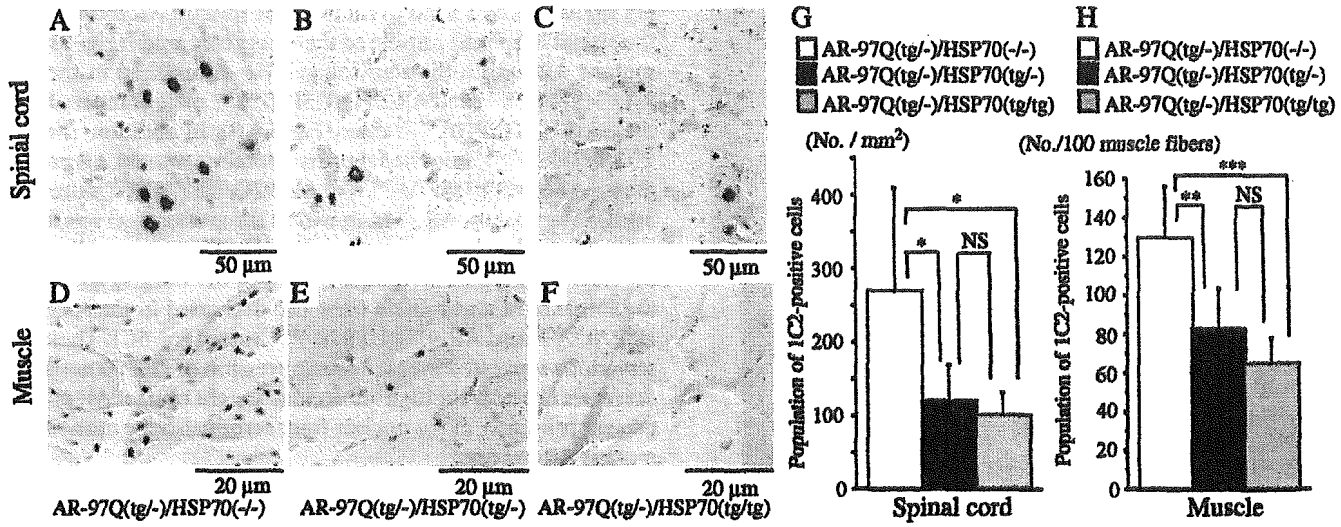

Figure 4. HSP70 decreases nuclear-localized mutant AR in double-transgenic mice. Immunohistochemical study of the spinal anterior horn (*A–C*) and muscle (*D–F*) of AR-97Q/HSP70$^{(-/-)}$ and AR-97Q/HSP70 double-transgenic mice stained with a monoclonal antibody (1C2) against abnormally expanded polyQ (16 weeks old). AR-97Q/HSP70$^{(-/-)}$ mice have intense and frequent staining for 1C2 in the nucleus (*A, D*). AR-97Q/HSP70$^{(tg/-)}$ (*B, E*), and AR-97Q/HSP70$^{(tg/tg)}$ (*C, F*) mice exhibit low levels of 1C2 staining in the nucleus. *G, H*, Quantitative assessment of diffuse nuclear staining for 1C2 in the spinal ventral horn (*G*) and muscle (*H*). Positively stained nuclei were estimated by counting in the thoracic spinal ventral horn and muscle using six transgenic mice (16 weeks of age). There are significantly more 1C2-positive cells in AR-97Q/HSP70$^{(-/-)}$ mice than in AR-97Q/HSP70$^{(tg/-)}$ mice or AR-97Q/HSP70$^{(tg/tg)}$ mice in both tissues. Results are expressed as means ± SD for six mice. The differences in 1C2-positive cell populations are not statistically significant between AR-97Q/HSP70$^{(tg/-)}$ and AR-97Q/HSP70$^{(tg/tg)}$ mice. $^{*}p < 0.05$; $^{**}p < 0.01$; $^{***}p < 0.001$.

genic mice, whereas testosterone administration enhanced the nuclear localization of mutant AR and caused significant motor dysfunction in the female transgenic mice (Katsuno et al., 2002). In particular, the large aggregated complexes of the mutant AR protein detected in the stacking gel or slowly migrating species in the Western blot analysis in the nuclear fraction were well correlated with the phenotypic expression in this mouse model (Katsuno et al., 2002). This suggested that oligomeric or polymeric mutant AR large complex molecules positively associated with other molecules would exert the toxicity rather than monomeric mutant AR (Katsuno et al., 2002).

In the present study, we demonstrated that the amount of nuclear-localized mutant AR protein, particularly that of the large complex form present in the stacking gel or trapped by the cellulose acetate membrane, was significantly reduced in the AR-97/HSP70 double-transgenic mice. Thus, the overexpression of HSP70 is suggested to exert its amelioration of the phenotypic expression by diminishing the amount of nuclear-localized mutant AR protein. However, in the previously reported SCA1 transgenic mouse model, NIs of the mutant protein were not apparently decreased in the double-transgenic mice with rat HSP70 overexpression, although the neurological deficit and neuronal degeneration were ameliorated (Cummings et al., 2001). Because the gain of amelioration for phenotypic expression in the model mice of Cummings et al. (2001) was mild even in the double-transgenics with HSP70 homozygotes, the change in the frequency of the NIs would not have been significant enough to detect. In our mouse model, NIs were present only in the small subpopulation of neurons and muscles, particularly in the early phase of phenotypic expression, whereas the 1C2-positive nuclei were abundant (Katsuno et al., 2002). In addition, 1C2-positive neurons are more extensive than those of NI-bearing neurons in the tissues of the autopsied samples from patients with polyQ diseases, and the distribution of 1C2-positive neurons is well correlated with the neurological symptoms (Yamada et al., 2001). These observations suggest that 1C2 staining is a more sensitive histological marker for the detection of the nuclear localization of the mutant protein with an expanded polyQ stretch compared with NIs detected by antibodies for the responsible protein.

The interesting observation in our study was the diminution of monomeric mutant AR in the double-transgenic mice with overexpression of HSP70. Recently, HSP70 overexpression in the cell culture model has revealed enhanced solubility of mutant AR with an expanded polyQ and degradation through the ubiquitin–proteasome system (Bailey et al., 2002). Overexpression of chaperones generally enhances the function of the ubiquitin–proteasome pathway and subsequently accelerates protein degradation (Bukau and Horwich, 1998). The ubiquitin–proteasome pathway, particularly its activity, is known to be related to chaperone expression levels (Bukau and Horwich, 1998). The molecular mechanism for this relationship remains unsolved, but recently CHIP (C terminal of HSC70-interacting protein), U-box-type E3 ubiquitin ligase, has been shown to interact with HSP90 or HSP70 (Connel et al., 2001) and ubiquitylate unfolded proteins trapped by molecular chaperones and degrades them, thus acting as a "quality control E3" (Murata et al., 2001). Furthermore, there is a cofactor of HSC70/HSP70, Bcl-2 associated athanogene 1, which possesses a ubiquitin-like domain and promotes binding of HSC70/HSP70 to the proteolytic complex (Lüders et al., 2000). Although such coupling factors between the HSP70 chaperone system and the protein degradation machinery for mutant AR are unknown at present, if the similar E3 for mutant AR is present, it could ubiquitylate and degrade mutant AR as a result of interacting with HSP70. In this scenario, the overexpression of HSP70 may accelerate E3-dependent capture of mutant AR and its degradation through the proteasome pathway. A remarkable reduction of the monomeric mutant AR in the double-transgenics with HSP70 overexpression can be the reflection of the accelerated degradation of mutant AR through the HSP70-mediated E3–proteasome system. Interaction between mutant AR and HSP70 detected by coimmunoprecipitation and Western blot analysis in the double-transgenic mice would support this view. The overexpression of HSP70 could enhance the degradation of the mo-

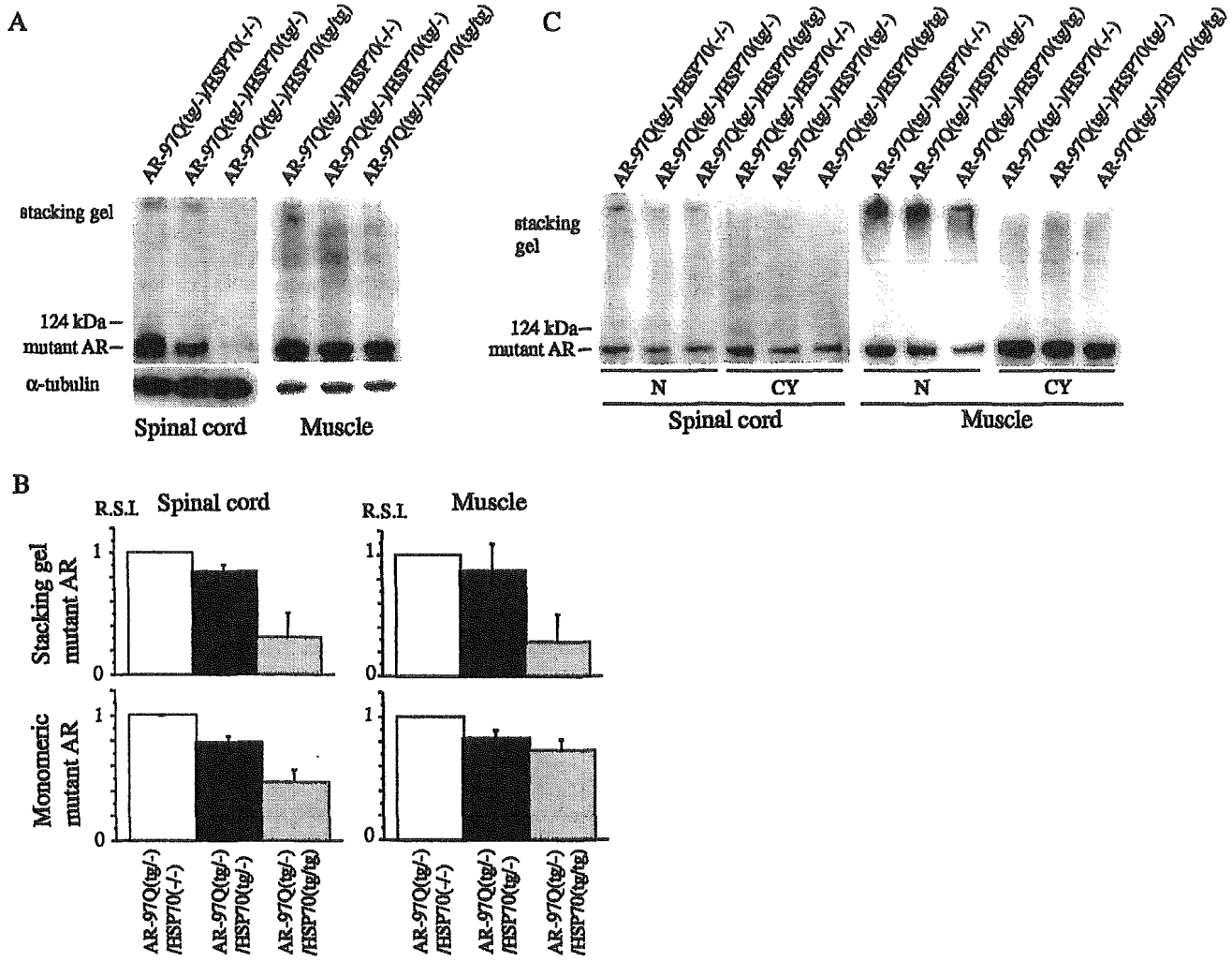

Figure 5. HSP70 decreases nuclear-localized mutant AR protein complexes as well as monomeric mutant AR. *A*, *B*, Western blot analysis of total tissue homogenates from the spinal cord and muscle of AR-97Q/HSP70$^{(-/-)}$, AR-97Q/HSP70$^{(tg/-)}$, and AR-97Q/HSP70$^{(tg/tg)}$ mice (16 weeks of age) immunolabeled by an antibody against AR (N-20). The mutant AR appearing within the stacking gel and monomeric mutant AR were diminished in AR-97Q/HSP70$^{(tg/-)}$ and AR-97Q/HSP70$^{(tg/tg)}$ mice compared with AR-97Q/HSP70$^{(-/-)}$ mice (*A*, *B*). Values of mutant AR were normalized to endogenous α-tubulin and expressed as the ratio to those of AR-97Q/HSP70$^{(-/-)}$ mice (*B*). Values are expressed as means ± SD for three mice. *C*, Western blot analysis of nuclear (*N*) and cytoplasmic (*CY*) fractions from the spinal cord and muscle of AR-97Q/HSP70$^{(-/-)}$, AR-97Q/HSP70$^{(tg/-)}$, and AR-97Q/HSP70$^{(tg/tg)}$ mice (16 weeks of age) immunolabeled by N-20. Mutant AR protein within the stacking gel was found primarily in the nuclear fraction. The mutant AR within the stacking gel of the nuclear fraction also significantly decreased in the spinal cord and muscle of AR-97Q/HSP70$^{(tg/tg)}$ mice. *R.S.I.*, Relative signal intensity.

nomeric mutant AR, presumably through the HSP70-interacting quality control E3 activation, and subsequently it could reduce the amount of nuclear-localized mutant AR, resulting in the amelioration of phenotypic expression induced by mutant AR. To substantiate this, however, one needs to identify the HSP70-interacting E3 ligase, which recognizes mutant AR as a substrate.

Another possibility is that overexpressed HSP70 directly renaturates the misfolded mutant AR and normalizes the interaction of mutant AR with proteins that are essential to maintain the cell function (Hendricks and Hartl, 1993). The overexpression of HSP70 and HSP40 or HSC70 and *Drosophila* human DNAJ homolog-1 (dHdj-1) changed the distribution and morphologic pattern of NI formation of mutant huntingtin and ataxin-1 (Cummings et al., 1998; Fernandez-Funez et al., 2000; Muchowski et al., 2000). The overexpression of dHdj-1 and HSP70 increased the proportion of the monomeric mutant protein with an expanded polyQ, suggesting that chaperones modulate the biochemical properties of mutant polyQ-bearing protein (Chan et al., 2000). It has been proposed that the disease proteins with an expanded polyQ participate in inappropriate protein–protein interactions that lead to cell dysfunction and eventual cell death (Sherman and Goldberg, 2001). Molecular chaperones can be involved in the conformational modification by stabilizing the unfolded mutant proteins and can facilitate or inhibit the interaction with self or other proteins (Opal and Zoghbi, 2002). To date, a number of proteins that interact with polyQ-bearing disease protein have been cloned, including huntingtin-associated protein (Li et al., 1995), huntingtin-interacting protein (Kalchman et al., 1997), glyceraldehyde-3-phosphate dehydrogenase (Burke et al., 1996), leucine-rich acidic nuclear protein (Matilla et al., 1997), polyglutamine tract-binding protein-1 (Waragai et al., 1999), 130 kDa human TATA-binding protein-associated factor subunit of the human transcription factor TFIID (Shimohata et al., 2000), and cAMP response element-binding protein (CREB) binding protein (CBP) (Nucifora et al., 2001; Zander et al., 2001). CBP has been demonstrated to interact with mutant AR, colocalize in the NIs, and reduce the mutant AR-induced cell toxicity by CBP overexpression in the cell culture model by modifying CBP-dependent transcriptional activity (McCampbell et al., 2000). HSP70 may reduce the toxicity of

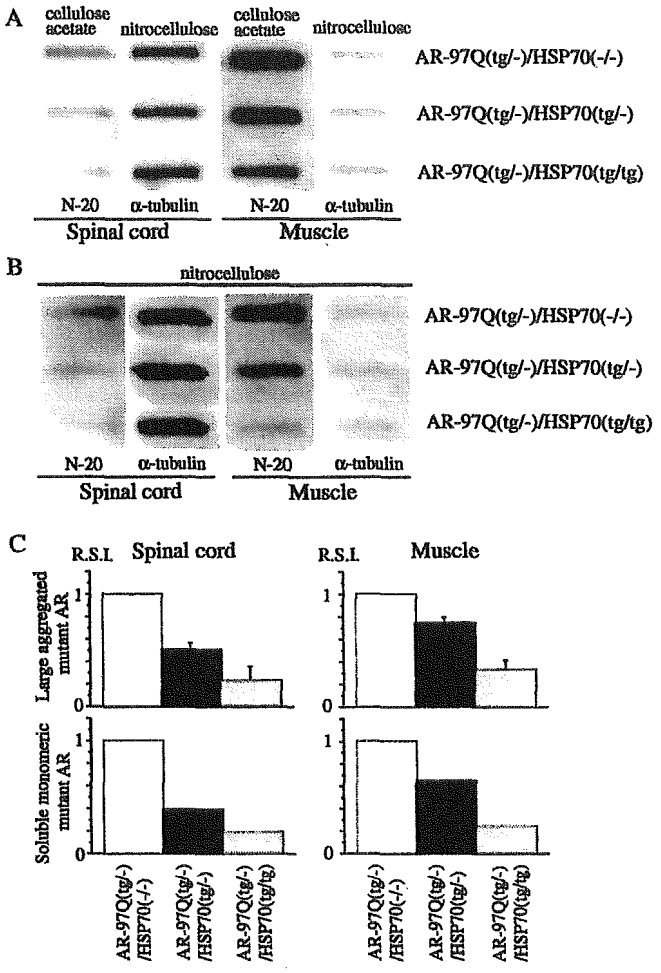

Figure 6. HSP70 decreases large aggregated mutant AR protein and soluble monomeric mutant AR protein. *A–C*, Filter-trap assay of total tissue homogenates from the spinal cord and muscle of AR-97Q/HSP70$^{(-/-)}$, AR-97Q/HSP70$^{(tg/-)}$, and AR-97Q/HSP70$^{(tg/tg)}$ mice (16 weeks of age) immunolabeled by an antibody against AR (N-20). Large aggregated mutant AR complexes were trapped by the cellulose acetate membrane (*A*), and soluble monomeric mutant AR passing through the cellulose acetate membrane was trapped by the nitrocellulose membrane beneath the cellulose acetate membrane (*B*). Endogenous α-tubulin using the nitrocellulose membrane was also shown (*A*, *B*). The normalized value of large aggregated mutant AR and soluble monomeric mutant AR against endogenous α-tubulin is shown in *C*. Relative values against those of AR-97Q/HSP70$^{(-/-)}$ mice were expressed as means ± SD for three mice or a mean of two mice (*C*). The trapped AR protein was reduced in the spinal cord and muscle of AR-97Q/HSP70$^{(tg/-)}$ and AR-97Q/HSP70$^{(tg/tg)}$ mice in both membranes (*A*, *B*). This reduction was most evident in AR-97Q/HSP70$^{(tg/tg)}$ mice (*A–C*), suggesting that the overexpression of HSP70 resulted in a significant, dose-dependent decrease in large aggregated and soluble monomeric mutant AR protein. *R.S.I.*, Relative signal intensity.

mutant AR proteins through the inhibition or acceleration of the interaction with these proteins. However, interacting protein involvement in association with mutant AR still needs to be investigated.

The other possible avenue by which HSP70 acts to improve polyQ-induced toxicity is the anti-apoptotic activities of HSP70. HSP70 suppresses apoptosis by inhibiting the *c*-Jun N-terminal kinase (Gabai et al., 1998) or by inhibiting cytochrome *c* release and caspase-3 activation (Li et al., 2000; Jana et al., 2001). Furthermore, HSP40 and mammalian relative of DNAJ chaperones can inhibit caspase-3 and caspase-9 activation mediated by mutant huntingtin, independent of huntingtin aggregation (Zhou et al., 2001; Chuang et al., 2002). However, the involvement of anti-apoptotic activities of HSPs in protection against mutant AR toxicity through reducing the nuclear-localized mutant AR remains to be elucidated.

In summary, the overexpression of HSP70 significantly ameliorates the phenotypes of SBMA transgenic mice by reducing the amount of nuclear-localized mutant AR protein, particularly that of the large complex form. The amount of monomeric mutant AR was also reduced by HSP70 overexpression, suggesting enhanced degradation of mutant AR. A recent study revealed that the ansamycin antibiotic Geldanamycin induced a heat shock response and inhibited aggregation of mutant huntingtin in COS-1 cells (Sittler et al., 2001). Thus, HSP70 overexpression would provide a potential therapeutic avenue for SBMA and other polyQ diseases.

References

Adachi H, Kume A, Li M, Nakagomi Y, Niwa H, Do J, Sang C, Kobayashi Y, Doyu M, Sobue G (2001) Transgenic mice with an expanded CAG repeat controlled by the human AR promoter show polyglutamine nuclear inclusions and neuronal dysfunction without neuronal cell death. Hum Mol Genet 10:1039–1048.

Bailey CK, Andriola IF, Kampinga HH, Merry DE (2002) Molecular chaperones enhance the degradation of expanded polyglutamine repeat androgen receptor in a cellular model of spinal and bulbar muscular atrophy. Hum Mol Genet 11:515–523.

Bukau KT, Horwich AL (1998) The Hsp70 and Hsp60 chaperone machines. Cell 92:351–366.

Burke JR, Enghild JJ, Martin ME, Jou YS, Myers RM, Roses AD, Vance JM, Strittmatter WJ (1996) Huntingtin and DRPLA proteins selectively interact with the enzyme GAPDH. Nat Med 2:347–350.

Carmichael J, Chatellier J, Woolfson A, Milstein C, Fersht AR, Rubinsztein DC (2000) Bacterial and yeast chaperones reduce both aggregate formation and cell death in mammalian cell models of Huntington's disease. Proc Natl Acad Sci USA 97:9701–9705.

Chai Y, Koppenhafer SL, Bonini NM, Paulson HL (1999) Analysis of the role of heat shock protein (Hsp) molecular chaperones in polyglutamine disease. J Neurosci 19:10338–10347.

Chan HYE, Warrick JM, Gray-Board GL, Paulson HL, Bonini NM (2000) Mechanisms of chaperone suppression of polyglutamine disease: selectivity, synergy and modulation of protein solubility in *Drosophila*. Hum Mol Genet 9:2811–2820.

Chuang JZ, Zhou H, Zhu M, Li SH, Li XJ, Sung CH (2002) Characterization of a brain-enriched chaperone, MRJ, that inhibits Huntingtin aggregation and toxicity independently. J Biol Chem 277:19831–19838.

Connel P, Ballinger CA, Jiang J, Wu Y, Thompson LJ, Höfeld J, Patterson C (2001) The co-chaperone CHIP regulates protein triage decisions mediated by heat shock proteins. Nat Cell Biol 3:93–96.

Cummings CJ, Mancini MA, Antalffy B, DeFranco DB, Orr HT, Zoghbi HY (1998) Chaperone suppression of aggregation and altered subcellular proteasome localization imply protein misfolding in SCA1. Nat Genet 19:148–154.

Cummings CJ, Sun Y, Opal P, Antalffy B, Mestril R, Orr HT, Dillmann WH, Zoghbi HY (2001) Overexpression of inducible HSP70 chaperone suppresses neuropathology and improves motor function in SCA1 mice. Hum Mol Genet 10:1511–1518.

Doyu M, Sobue G, Mukai E, Kachi T, Yasuda T, Mitsuma T, Takahashi A (1992) Severity of X-linked recessive bulbospinal neuronopathy correlates with size of the tandem CAG repeat in androgen receptor gene. Ann Neurol 23:707–710.

Fernandez-Funez P, Nino-Rosales ML, de Gouyon B, She WC, Luchak JM, Martinez P, Turiegano E, Benito J, Capovilla M, Skinner PJ, McCall A, Canal I, Orr HT, Zoghbi HY, Botas J (2000) Identification of genes that modify ataxin-1-induced neurodegeneration. Nature 408:101–106.

Gabai VL, Meriin AB, Yaglom JA, Volloch VZ, Sherman MY (1998) Role of Hsp70 in regulation of stress-kinase JNK: implications in apoptosis and aging. FEBS Lett 438:1–4.

Hendricks JP, Hartl FU (1993) Molecular chaperone functions of heat-shock proteins. Annu Rev Biochem 62:349–384.

Huynh DP, Figueroa K, Hoang N, Pulst SM (2000) Nuclear localization or inclusion body formation of ataxin-2 are not necessary for SCA2 pathogenesis in mouse or human. Nat Genet 26:44–50.

Igarashi S, Tanno Y, Onodera O, Yamazaki M, Sato S, Ishikawa A, Miyatani N, Nagashima M, Ishikawa Y, Sahashi K, Ibi T, Miyatake T, Tsuji S (1992)

Strong correlation between the number of CAG repeats in androgen receptor genes and the clinical onset of features of spinal and bulbar muscular atrophy. Neurology 42:2300–2302.

Jana NR, Tanaka M, Wang GH, Nukina N (2000) Polyglutamine length-dependent interaction of Hsp40 and Hsp70 family chaperones with truncated N-terminal huntingtin: their role in suppression of aggregation and cellular toxicity. Hum Mol Genet 9:2009–2018.

Jana NR, Zemskov EA, Wang GH, Nukina N (2001) Altered proteasomal function due to the expression of polyglutamine-expanded truncated N-terminal huntingtin induces apoptosis by caspase activation through mitochondrial cytochrome c release. Hum Mol Genet 10:1049–1059.

Kalchman MA, Koide HB, McCutcheon K, Graham RK, Nichol K, Nishiyama K, Kazemi-Esfarjani P, Lynn FC, Wellington C, Metzler M, Goldberg YP, Kanazawa I, Gietz RD, Hayden MR (1997) HIP1, a human homologue of *S. cerevisiae* Sla2p, interacts with membrane-associated huntingtin in the brain. Nat Genet 16:44–53.

Katsuno M, Adachi H, Kume A, Li M, Nakagomi Y, Niwa H, Sang C, Kobayashi Y, Doyu M, Sobue G (2002) Testosterone reduction prevents phenotypic expression in a transgenic mouse model of spinal and bulbar muscular atrophy. Neuron 35:843–854.

Kennedy WR, Alter M, Sung JH (1968) Progressive proximal spinal and bulbar muscular atrophy of late onset: a sex-linked recessive trait. Neurology 18:671–680.

Kobayashi Y, Sobue G (2001) Protective effect of chaperones on polyglutamine diseases. Brain Res Bull 56:165–168.

Kobayashi Y, Kume A, Li M, Doyu M, Hata M, Ohtsuka K, Sobue G (2000) Chaperones Hsp70 and Hsp40 suppress aggregate formation and apoptosis in cultured neuronal cells expressing truncated androgen receptor protein with expanded polyglutamine tract. J Biol Chem 275:8772–8778.

La Spada AR, Roling DB, Harding AE, Warner CL, Spiegel R, Hausmanowa-Petrusewicz I, Yee WC, Fischbeck KH (1992) Meiotic stability and genotype-phenotype correlation of the trinucleotide repeat in X-linked spinal and bulbar muscular atrophy. Nat Genet 2:301–304.

Li CY, Lee JS, Ko YG, Kim JI, Seo JS (2000) Heat shock protein 70 inhibits apoptosis downstream of cytochrome c release and upstream of caspase-3 activation. J Biol Chem 275:25665–25671.

Li M, Miwa S, Kobayashi Y, Merry DE, Tanaka F, Doyu M, Hashizume Y, Fischbeck KH, Sobue G (1998a) Nuclear inclusions of the androgen receptor protein in spinal and bulbar muscular atrophy. Ann Neurol 44:249–254.

Li M, Nakagomi Y, Kobayashi Y, Merry DE, Tanaka F, Doyu M, Mitsuma T, Fischbeck KH, Sobue G (1998b) Nonneural nuclear inclusions of androgen receptor protein in spinal and bulbar muscular atrophy. Am J Pathol 153:695–701.

Li XJ, Li SH, Sharp AH, Nucifora Jr FC, Schilling G, Lanahan A, Worley P, Snyder SH, Ross CA (1995) A huntingtin-associated protein enriched in brain with implications for pathology. Nature 378:398–402.

Lüders J, Demand J, Höhfeld J (2000) The ubiquitin-related BAG-1 provides a link between the molecular chaperones Hsc70/Hsp70 and the proteasome. J Biol Chem 275:4613–4617.

Matilla A, Koshy BT, Cummings CJ, Isobe T, Orr HT, Zoghbi HY (1997) The cerebellar leucine-rich acidic nuclear protein interacts with ataxin-1. Nature 389:974–978.

McCampbell A, Taylor JP, Taye AA, Robitschek J, Li M, Walcott J, Merry D, Chai Y, Paulson H, Sobue G, Fischbeck KH (2000) CREB-binding protein sequestration by expanded polyglutamine. Hum Mol Genet 9:2197–2202.

Muchowski PJ, Schaffar G, Sittler A, Wanker EE, Hayer-Hartl MK, Hartl FU (2000) Hsp70 and hsp40 chaperones can inhibit self-assembly of polyglutamine proteins into amyloid-like fibrils. Proc Natl Acad Sci USA 97:7841–7846.

Murata S, Minami Y, Minami M, Chiba T, Tanaka K (2001) CHIP is a chaperone-dependent E3 ligase that ubiquitylates unfolded protein. EMBO Rep 2:1133–1138.

Nucifora Jr FC, Sasaki M, Peters MF, Huang H, Cooper JK, Yamada M, Takahashi H, Tsuji S, Troncoso J, Dawson VL, Dawson TM, Ross CA (2001) Interference by huntingtin and atrophin-1 with cbp-mediated transcription leading to cellular toxicity. Science 291:2423–2428.

Opal P, Zoghbi HY (2002) The role of chaperones in polyglutamine disease. Trends Mol Med 8:232–236.

Plumier JC, Ross BM, Currie RW, Angelidis CE, Kaziaris H, Kollias G, Pagoulatos GN (1995) Transgenic mice expressing the human heat shock protein 70 have improved post-ischemic myocardial recovery. J Clin Invest 95:1854–1860.

Ross CA (2002) Polyglutamine pathogenesis: emergence of unifying mechanisms for Huntington's disease and related disorders. Neuron 35:819–822.

Schmidt T, Lindenberg KS, Krebs A, Schols L, Laccone F, Herms J, Rechsteiner M, Riess O, Landwehrmeyer GB (2002) Protein surveillance machinery in brains with spinocerebellar ataxia type 3: redistribution and differential recruitment of 26S proteasome subunits and chaperones to neuronal intranuclear inclusions. Ann Neurol 51:302–310.

Sherman MY, Goldberg AL (2001) Cellular defenses against unfolded proteins: a cell biologist thinks about neurodegenerative diseases. Neuron 29:15–32.

Shimohata T, Nakajima T, Yamada M, Uchida C, Onodera O, Naruse S, Kimura T, Koide R, Nozaki K, Sano Y, Ishiguro H, Sakoe K, Ooshima T, Sato A, Ikeuchi T, Oyake M, Sato T, Aoyagi Y, Hozumi I, Nagatsu T, et al. (2000) Expanded polyglutamine stretches interact with TAFII130,interfering with CREB-dependent transcription. Nat Genet 26:29–36.

Sittler A, Lurz R, Lueder G, Priller J, Hayer-Hartl MK, Hartl FU, Lehrach H, Wanker EE (2001) Geldanamycin activates a heat shock response and inhibits huntingtin aggregation in a cell culture model of Huntington's disease. Hum Mol Genet 10:1307–1315.

Sobue G, Hashizume Y, Mukai E, Hirayama M, Mitsuma T, Takahashi A (1989) X-linked recessive bulbospinal neuronopathy: a clinicopathological study. Brain 112:209–232.

Stenoien DL, Cummings CJ, Adams HP, Mancini MG, Patel K, DeMartino GN, Marcelli M, Weigel NL, Mancini MA (1999) Polyglutamine-expanded androgen receptors form aggregates that sequester heat shock proteins,proteasome components and SRC-1,and are suppressed by the HDJ-2 chaperone. Hum Mol Genet 8:731–741.

Takahashi A (2001) Hiroshi Kawahara (1858–1918). J Neurol 248:241–242.

Tanaka F, Doyu M, Ito Y, Matsumoto M, Mitsuma T, Abe K, Aoki M, Itoyama Y, Fischbeck KH, Sobue G (1996) Founder effect in spinal and bulbar muscular atrophy (SBMA). Hum Mol Genet 5:1253–1257.

Tanaka F, Reeves MF, Ito Y, Matsumoto M, Li M, Miwa S, Inukai A, Yamamoto M, Doyu M, Yoshida M, Hashizume Y, Terao S, Mitsuma T, Sobue G (1999) Tissue-specific somatic mosaicism in spinal and bulbar muscular atrophy (SBMA) is dependent on CAG repeat length and androgen receptor gene expression level. Am J Hum Genet 65:966–973.

Terao S, Sobue G, Hashizume Y, Li M, Inagaki T, Mitsuma T (1996) Age-related changes in human spinal ventral horn cells with special reference to the loss of small neurons in the intermediate zone: a quantitative analysis. Acta Neuropathol (Berl) 92:109–114.

Waelter S, Boeddrich A, Lurz R, Scherzinger E, Lueder G, Lehrach H, Wanker EE (2001) Accumulation of mutant huntingtin fragments in aggresome-like inclusion bodies as a result of insufficient protein degradation. Mol Biol Cell 12:1393–1407.

Wanker EE, Scherzinger E, Heiser V, Sittler A, Eickhoff H, Lehrach H (1999) Membrane filter assay for detection of amyloid-like polyglutamine-containing protein aggregates. Methods Enzymol 309:375–386.

Waragai M, Lammers C, Takeuchi S, Imafuku I, Udagawa Y, Kanazawa I, Kawabata M, Mouradian MM, Okazawa H (1999) PQBP-1,a novel polyglutamine tract-binding protein,inhibits transcription activation by Brn-2 and affects cell survival. Hum Mol Genet 8:977–987.

Warrick JM, Chan HY, Gray-Board GL, Chai Y, Paulson HL, Bonini NM (1999) Suppression of polyglutamine-mediated neurodegeneration in *Drosophila* by the molecular chaperone HSP70. Nat Genet 23:425–428.

Yamada M, Wood JD, Shimohata T, Hayashi S, Tsuji S, Ross CA, Takahashi H (2001) Widespread occurrence of intranuclear atrophin-1 accumulation in the central nervous system neurons of patients with dentatorubral-pallidoluysian atrophy. Ann Neurol 49:14–23.

Zander C, Takahashi J, Hachimi KHE, Fujigasaki H, Albanese V, Lebre AS, Stevanin G, Duyckaerts C, Brice A (2001) Similarities between spinocerebellar ataxia type 7 (SCA7) cell models and human brain: proteins recruited in inclusions and activation of caspase-3. Hum Mol Genet 10:2569–2579.

Zhou H, Li SH, Li XJ (2001) Chaperone suppression of cellular toxicity of huntingtin is independent of polyglutamine aggregation. J Biol Chem 276:48417–48424.

Zoghbi HY, Orr HT (2000) Glutamine repeats and neurodegeneration. Annu Rev Neurosci 23:217–247.

Reprinted from JOURNAL OF NEUROLOGY, NEUROSURGERY & PSYCHIATRY, April 2003, Vol 74, No 4, p 419-422

PAPER

Occipital hypoperfusion in Parkinson's disease without dementia: correlation to impaired cortical visual processing

Y Abe, T Kachi, T Kato, Y Arahata, T Yamada, Y Washimi, K Iwai, K Ito, N Yanagisawa, G Sobue

J Neurol Neurosurg Psychiatry 2003;74:419–422

See end of article for authors' affiliations

Correspondence to: Dr Y Abe, Department of Neurology, Chubu National Hospital, Obu, Aichi 474-8511, Japan; yujiabe@chubu-nh.go.jp

Received 5 August 2002
Accepted in revised form 22 October 2002

Objective: The purpose of this study was to analyse changes in regional cerebral blood flow (rCBF) in Parkinson's disease (PD) without dementia.
Methods: Twenty eight non-demented patients with PD and 17 age matched normal subjects underwent single photon emission computed tomography with N-isopropyl-p-[^{123}I]iodoamphetamine to measure rCBF. The statistical parametric mapping 96 programme was used for statistical analysis.
Results: The PD patients showed significantly reduced rCBF in the bilateral occipital and posterior parietal cortices ($p<0.01$, corrected for multiple comparison $p<0.05$), when compared with the control subjects. There was a strong positive correlation between the score of Raven's coloured progressive matrices (RCPM) and the rCBF in the right visual association area ($p<0.01$, corrected for multiple comparison $p<0.05$) among the PD patients.
Conclusions: This study showed occipital and posterior parietal hypoperfusion in PD patients without dementia. Furthermore, it was demonstrated that occipital hypoperfusion is likely to underlie impairment of visual cognition according to the RCPM test, which is not related to motor impairment.

It has been reported in previous studies that patients with Parkinson's disease (PD), even those without dementia, showed changes in regional cerebral blood flow (rCBF).[1–8] However, the findings of these investigations have been inconsistent. Frontal[1 2] parietal,[3], temporal,[4] or global[1 5] cortical hypoperfusion, or unchanged blood flow[6–8] have been reported. This inconsistency is considered to be attributable, not only to the heterogeneity among PD patients, but also to the lack of standardisation of image-analysing methods. In most previous studies, visually placed region of interest (ROI) analysis methods were used to evaluate the alterations of rCBF. This approach is limited in that the manual placement of ROI gives rise to the observer biases and large areas of the brain are left unexplored.

Statistical parametric mapping (SPM), developed by Frinston *et al*, is a voxel based statistical technique that is used to examine regional changes in imaging data.[9 10] This is entirely automated and objective, and can completely overcome the disadvantage of earlier ROI analysis methods. Recently, the SPM programme has been widely used to examine regional dysfunction of the brain in various neurological diseases.[5 11–13]

The purpose of this study was to analyse the rCBF in PD patients without dementia on a voxel by voxel basis using single photon emission computed tomography (SPECT) with N-isopropyl-p-[^{123}I]iodoamphetamine (^{123}I-IMP) and the SPM programme. We compared the rCBF in PD patients to that in age matched normal subjects. In addition, we investigated the relation between the rCBF and clinical features in PD patients.

Table 1 Clinical features of subjects

	Normal controls (n=17)	Patients with Parkinson's disease (n=28)
Age (y)*	69.6(10.2)	67.3 (7.3)
Sex (F/M)	9/8	17/11
Duration of illness (y)*		8.6 (4.6)
UPDRS motor score*		35.2 (12.9)

*Mean (SD).

METHODS

Subjects

Twenty eight PD patients without dementia and 17 age matched normal control subjects were included in this study (table 1). The 28 PD patients were diagnosed with the United Kingdom Parkinson's Disease Society Brain Bank criteria for clinical diagnosis of idiopathic PD,[14] and the extrapyramidal symptoms were scored according to the motor examination score of the Unified Parkinson's Disease Rating Scale (UPDRS).[15] Patients who had visual hallucination were excluded. No abnormal intensity or obvious cortical atrophy was seen on magnetic resonance imaging of the brain of any patient. None of the patients had any other illnesses or were taking any medication, except for antiparkinsonian drugs. All 28 patients had been taking levodopa treatment at the time of SPECT scanning. In addition, dopamine receptor agonists had been used in 12 patients, six patients had been treated with low dose anticholinergic agents, droxydopa had been given to two patients, and three patients had been taking amantadine hydrochloride.

None of the 17 normal control subjects had a history of any neurological or psychiatric disorders, and the neurological examination of each control subject was normal.

All of the PD and control subjects were assessed using the mini-mental state examination (MMSE),[16] and 25 PD patients and 14 control subjects also took the Raven's coloured progressive matrices (RCPM).[17] For both SPECT scanning and cognitive test, all patients were examined after overnight withdrawal of medication.

Informed consent was obtained from every subject before the study. Permission to perform this study was obtained from the ethical committee of Chubu National Hospital.

Abbreviations: PD, Parkinson's disease; rCBF, regional cerebral blood flow; RCPM, Raven's coloured progressive matrices; MMSE, mini-mental state examination; ROI, region of interest; SPM, statistical parametric mapping

Image acquisition

^{123}I-IMP (Nihon Mediphysics, Hyogo, Japan), 222 MBq (6 mCi), was injected into an antecubital vein while the subjects laid in a supine position with eyes closed in a quiet room. A single blood sample was obtained from the brachial artery between 9 and 10 minutes after the ^{123}I-IMP administration. SPECT scanning was carried out between 15 and 45 minutes after injection using a two head rotating GCA 7200DI gammacamera (Toshiba, Tokyo, Japan) fitted with low energy, high resolution collimators. The data were acquired in a 128×128 matrix through a 180° rotation at an angle interval of 4°. The projection data were prefiltered through a Butterworth filter, and then reconstructed using a Ramp backprojection filter. Chang's attenuation correction[18] and scattering correction using the triple energy window method[19] were applied to the reconstructed images. The in-plane spatial resolution was 11.1 mm in full width at half maximum (FWHM). The final image slices were set up parallel to the orbitomeatal line and were obtained at an interval of 3.44 mm through the entire brain. The rCBF images were quantitated according to the IMP-ARG method.[20] This method is based on the two compartment model for tracer kinetics, and uses a standard arterial input calibrated by the radioactivity of a single arterial whole blood sample, a standard lipophilic fraction of ^{123}I-IMP in whole blood and fixed distribution volume of ^{123}I-IMP. All images were transferred to a Sun workstation (Sun Microsystems, Mountain View, CA, USA) for further analysis.

Data analysis

The data were analysed using the statistical parametric mapping 96 (SPM96; Wellcome Department of Cognitive Neurology, Institute of Neurology, London, UK)[9 10] implemented in MATLAB (Math Works, Sherborn, MA, USA). Each image was transformed into the standard anatomical space with the programme provided by the Montreal Neurological Institute.[21] All of the images resulting from the normalisation procedure were visually acceptable. The global CBF of PD patients was 49.5 (9.9) ml/100g/min (mean (SD)), and that of normal controls was 52.4 (13.1) ml/100g/min. There was no significant difference of the mean global CBF in the two groups, but the apparent interindividual variation of the global CBF was seen in each group. Therefore, in the following analyses, proportional scaling was applied to adjust the mean whole brain activity to 50 ml/100 g/min to avoid interindividual variation in global CBF. The grey matter threshold was 0.8.

For comparison between the PD group and the control group, the normalised images of the non-demented patients with PD and those of the normal subjects were compared by a voxel by voxel *t* statistics. The resulting statistical parametric maps of *t* statistics, SPM{t}, were transformed to maps of the unit normal distribution, SPM{z}. The statistical significance was chosen at a level of $z>2.33$ (equivalent to an uncorrected $p<0.01$). To correct for multiple comparisons, the significance of the difference between each detected brain region was estimated using distributional approximations from theory of Gaussian field, in terms of spatial extent and peak height. A corrected p value of 0.05 was used as the final threshold for significance.

Next, we compared the images of the PD patients to examine whether there were any voxels in which the rCBF was significantly correlated with various clinical characteristics including the duration of illness, the UPDRS motor score, the MMSE score, and the RCPM score. Each value of the clinical characteristics was used as a covariate of interest, and both the values of the global rCBF and age were used as confounding covariates. The statistical significance was chosen at a level of $z>2.33$ (equivalent to an uncorrected $p<0.01$). A corrected p value of 0.05 was chosen in multiple comparisons.

Table 2 Brain regions in which the rCBF of the PD group was significantly lower than that of the normal control group (SPM analysis)

Cerebral region	Brodmann's area	x	y	z	Z
L middle occipital gyrus	18, 19, 39	-34	-78	8	4.63
R middle occipital gyrus	18, 19, 39	28	-84	14	4.28
L angular gyrus	39	-46	-54	34	3.43
R angular gyrus	39	44	-56	38	3.98
L cuneus	18	-26	-86	0	3.37
R cuneus	18	8	-88	14	2.57
L calcarine sulcus	17	-18	-94	-8	3.69
L precuneus	7	-10	-70	42	3.37
L lingual gyrus	18	-18	-84	-16	3.36
L superior occipital gyrus	19	-32	-84	30	3.34
L superior parietal lobule	7	-12	-72	52	3.23

x, y, z=coodinates of the peak in the standard anatomical space; Z=Z score of maximal peak; L=left; R=right. $p<0.01$, corrected for multiple comparisons.

RESULTS

Clinical manifestations

The total UPDRS motor examination score ranged from 3 to 56, and the mean (SD) score was 34.8 (13.2). The mean MMSE score of the 28 PD patients was 28.1 (2.1) (range, 25 to 30), and that of the 17 control subjects was 28.5 (2.0) (range, 25 to 30). The MMSE score of the PD group did not differ significantly from that of the control group. The mean RCPM score was 24.4 (5.2) (range, 16 to 33) for the 25 PD patients, and was 28.2 (3.5) (range, 25 to 34) for the 10 control subjects. The RCPM score of the PD group was significantly lower than that of the control group ($p<0.05$).

There was no correlation between the age, the duration of illness, the UPDRS motor examination score, the MMSE score, and the RCPM score in the PD group.

Comparison of the rCBF between the PD and normal control groups

Twenty eight PD patients without dementia and 17 control subjects underwent SPECT scanning, and the images of the PD and control groups were compared. According to SPM analysis, the rCBF in the bilateral occipital cortices and the bilateral posterior parietal cortices in the PD group were significantly lower than those in the respective area in the control group ($p<0.01$, corrected $p<0.05$) (table 2, fig 1).

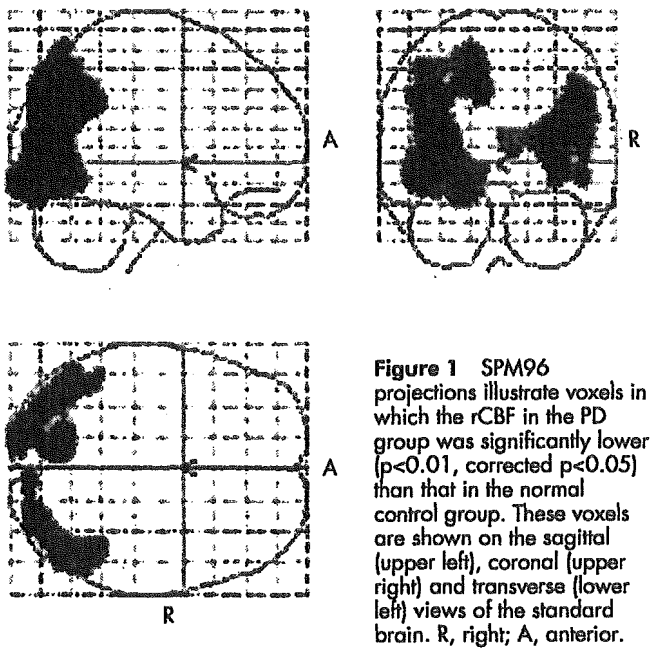

Figure 1 SPM96 projections illustrate voxels in which the rCBF in the PD group was significantly lower ($p<0.01$, corrected $p<0.05$) than that in the normal control group. These voxels are shown on the sagittal (upper left), coronal (upper right) and transverse (lower left) views of the standard brain. R, right; A, anterior.

Table 3 Brain regions in which there was a positive correlation between the RCPM score and the rCBF among 25 PD patients (SPM analysis)

Cerebral region	Brodmann's area	x	y	z	Z
R angular gyrus	39	46	-66	24	4.36
R middle occipital gyrus	19	40	-70	18	4.34
R inferior parietal lobule	40	42	-50	46	3.09

x, y, z=coodinates of the peak in the standard anatomical space; Z=Z score of maximal peak; R=right. p<0.01, corrected for multiple comparisons.

There was no brain region in which the rCBF was significantly higher in the PD group than in the control group.

Correlation between clinical characteristics and rCBF in the PD patients without dementia

There was a positive correlation between the RCPM score and the rCBF in the right dorsolateral occipital and the right posterior parietal cortices ($p<0.01$, corrected $p<0.05$) among 25 PD patients (table 3, fig 2). In most of these regions, the rCBF was reduced significantly in the PD group compared with the normal control group. There was no correlation between the duration of illness, the UPDRS motor examination score, or the MMSE score and the value of rCBF for any brain region.

DISCUSSION

This study showed that the rCBF in the non-demented PD patients was significantly lower than that in the age matched normal subjects in the bilateral occipital and posterior parietal cortices. It is well known that patients with PD, even those who do not have dementia, often develop various kinds of cognitive abnormalities that are closely related to visual dysfunction. Loss of luminance and colour contrast sensitivity and the impairment in preattentive cortical visual processing have been reported.[22-24] Furthermore, neuropsychological studies have revealed that PD patients have visuospatial deficit.[25 26] It seems appropriate to conclude that occipital dysfunction is a common feature of PD patients without dementia.

Actually, in our study, the mean RCPM score in the PD group was significantly lower than that in the normal control group, although the MMSE score of the PD group and that of the control group did not differ. RCPM is used for evaluation of visual perception, especially visuospatial attention, as the person taking the test must visually analyse form, colour, and linear slope.[27] Moreover, RCPM is one of the most appropriate batteries to test visual perceptual function purely, because it requires very little motor response. Therefore, in PD patients, the RCPM score is not likely to be affected by the poor motor ability. In fact, the RCPM score did not correlate to the UPDRS motor score in our PD patients. The impairment in RCPM test is clearly distinct from dementia, and is not considered to be secondary to the motor dysfunction.

In this study, we found that there was a strong positive correlation between the RCPM score and the rCBF in the right dorsolateral occipital area, corresponding to the visual association cortex, and the right posterior parietal area among non-demented PD patients. In these areas, there was no correlation between the UPDRS motor score and the rCBF, therefore, it may be reasonable to suppose that the reduction of rCBF in the visual association area purely reflects the impairment in cortical visual processing. Although some previous studies demonstrated occipital hypoperfusion and glucose hypometabolism,[5 28-31] there has been no previous study showing that the correlation between occipital hypometabolism or hypoperfusion and clinical abnormality related with visual

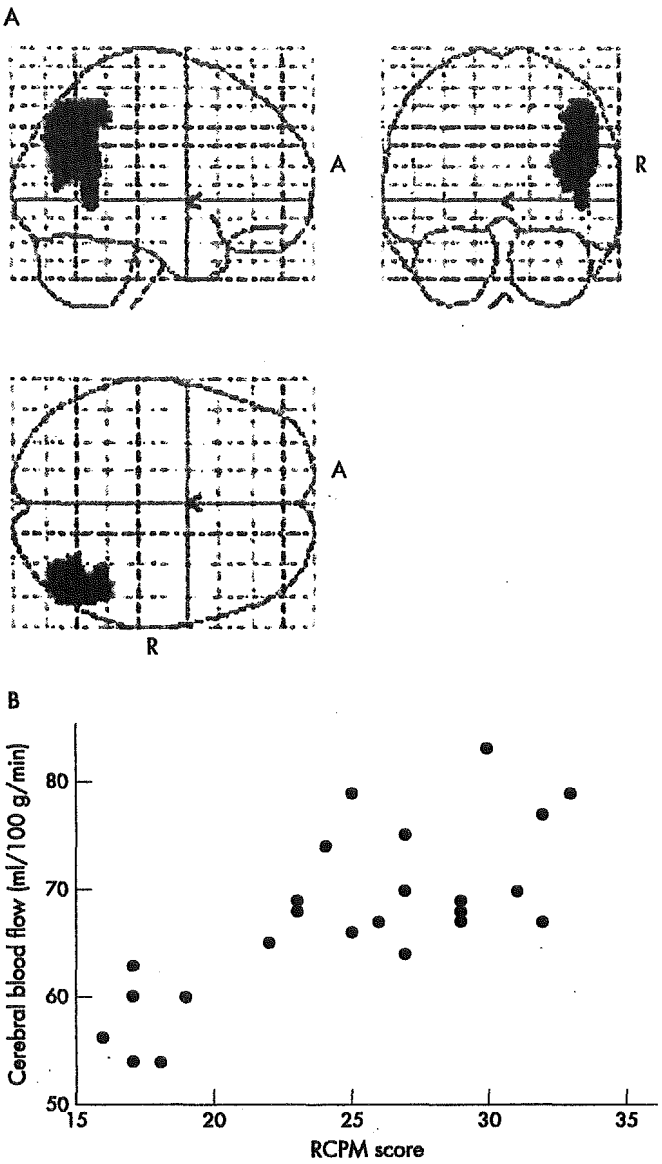

Figure 2 (A) SPM96 projections illustrate voxels in which there is a positive correlation ($p<0.01$, corrected $p<0.05$) between the RCPM score and the rCBF among 25 PD patients. R, right; A, anterior. (B) Scatter plot between the RCPM score and the rCBF at the voxel in the right middle occipital gyrus where there is a positive correlation ($p<0.005$, $r=0.73$, Spearman's correlation coefficient by ranks) between the RCPM score and the rCBF. *The mean whole brain activity was adjusted to 50 ml/100 g/min.

dysfunction was directly proved. This is the first study to demonstrate this correlation. The reason why the correlation was seen only in the right hemisphere is not clear, but this is possibly associated with the dominance of the right hemisphere in visuospatial attention.[32 33]

The underlying mechanism of the reduction of rCBF in the occipital lobe of PD patients remains unknown. In the previous report, a reduction of amplitude in the pattern electroretinogram[34] was demonstrated in PD patients. This abnormality has been considered to be attributable to diminished dopaminergic neurons in the retina, and this retinal dysfunction may be responsible for the occipital hypoperfusion. Furthermore, PD patients may have primary pathological findings in the cortices. However, morphological studies have not disclosed primary abnormalities, such as neuronal loss, gliosis, and appearance of Lewy bodies, in these brain regions in non-demented PD patients.[35 36] Another explanation, which seems much more plausible, is a functional deficit of the cortex that results from damage to the